

Orbital Symmetry Control of Electronic Coupling in a Symmetrical, All-Carbon-Bridged “Mixed Valence” Compound: Synthesis, Spectroscopy, and Electronic Structure of $[\{\text{Mo}(\text{dppe})(\eta\text{-C}_7\text{H}_7)\}_2(\mu\text{-C}_4)]^{n+}$ ($n = 0, 1, \text{ or } 2$)

Emma C. Fitzgerald,[†] Neil J. Brown,[‡] Ruth Edge,[§] Madeleine Helliwell,[†] Hannah N. Roberts,[†] Floriana Tuna,[†] Andrew Beeby,[‡] David Collison,[§] Paul J. Low,^{*,‡} and Mark W. Whiteley^{*,†}

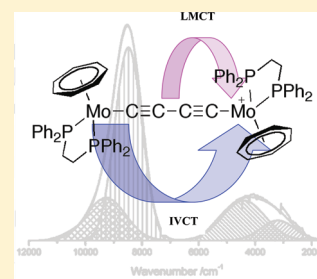
[†]School of Chemistry, University of Manchester, Manchester M13 9PL, U.K.

[‡]Department of Chemistry, Durham University, South Road, Durham, DH1 3LE, U.K.

[§]EPSRC National Service for EPR Spectroscopy, School of Chemistry, University of Manchester, Manchester, M13 9PL, U.K.

Supporting Information

ABSTRACT: The cycloheptatrienyl molybdenum alkynyl complex $[\text{Mo}(\text{C}\equiv\text{CH})(\text{dppe})(\eta\text{-C}_7\text{H}_7)]$, **1** ($\text{dppe} = \text{Ph}_2\text{PCH}_2\text{CH}_2\text{PPh}_2$), undergoes oxidative dimerization on reaction with $[\text{FeCp}_2]\text{PF}_6$ in thf at -78°C to give the bis(vinylidene) $[\{\text{Mo}(\text{dppe})(\eta\text{-C}_7\text{H}_7)\}_2(\mu\text{-C}=\text{CH}-\text{CH}=\text{C})][\text{PF}_6]_2$, **[2]** $[\text{PF}_6]_2$. Deprotonation of **[2]** $[\text{PF}_6]_2$ with KOBU^t yields butadiyndiyl-bridged $[\{\text{Mo}(\text{dppe})(\eta\text{-C}_7\text{H}_7)\}_2(\mu\text{-C}\equiv\text{C}-\text{C}\equiv\text{C})][\text{PF}_6]_2$, **[3]** $[\text{PF}_6]_2$, which undergoes *in situ* aerial oxidation to give $[\{\text{Mo}(\text{dppe})(\eta\text{-C}_7\text{H}_7)\}_2(\mu\text{-C}_4)][\text{PF}_6]_2$, **[3]** $[\text{PF}_6]_2$, as the major product. The cyclic voltammogram of **[3]** $[\text{PF}_6]_2$ exhibits a series of four redox processes indicative of sequential formation of $[\{\text{Mo}(\text{dppe})(\eta\text{-C}_7\text{H}_7)\}_2(\mu\text{-C}_4)]^{n+}$ ($n = 0, 1, 2, 3, 4$) with the comproportionation constant, K_C , for **[3]** $[\text{PF}_6]_2$ of 1.9×10^7 . Spectroscopic investigations on **[3]** $[\text{PF}_6]_2$ by IR, Raman, NIR, and EPR spectroscopy reveal properties characteristic of a d^5/d^6 mixed valence complex with a localized electronic structure and an estimated intramolecular electron transfer rate in the range $10^8\text{--}10^{10}\text{ s}^{-1}$. The experimental NIR spectrum of **[3]** $[\text{PF}_6]_2$ is consistent with the predicted spectral characteristics of a three-state model for bridge-mediated, electron transfer in a weakly coupled, symmetrical mixed valence system. The dication **[3]** $[\text{PF}_6]_2$ was isolated by chemical oxidation and structurally characterized; magnetic susceptibility measurements on **[3]** $[\text{PF}_6]_2$ in the temperature range 2–300 K reveal strong antiferromagnetic coupling with the exchange coupling constant J_{ab} (defined according to the Hamiltonian $\hat{H}_{\text{spin}} = -J_{ab}\hat{S}_a\hat{S}_b$) determined as $-406 (\pm 3)\text{ cm}^{-1}$.



INTRODUCTION

Diyndiyl-bridged bimetallic complexes $[\{\text{L}_x\text{M}\}\text{-C}\equiv\text{C}-\text{C}\equiv\text{C}-\{\text{ML}_x\}]$, in which redox-active metal end-caps $\{\text{ML}_x\}$ are linked by an unsaturated linear four-carbon chain bridge, have been at the forefront of investigations into the basic chemistry of metal-supported all-carbon molecules and as model systems for molecular wires.^{1–4} Complexes bearing a wide range of redox-active metal end-caps $\{\text{ML}_x\}$ have been investigated, including examples featuring $\text{Fe}(\text{dppe})\text{Cp}^*$,^{5,6} $\text{Re}(\text{NO})(\text{PPh}_3)\text{Cp}^*$,⁷ $\text{Ru}(\text{PP})\text{Cp}'$ [$\text{PP})\text{Cp}' = (\text{PPh}_3)_2\text{Cp}$,⁸ $(\text{dppe})\text{Cp}^*$,⁹ $(\text{dppf})\text{Cp}^{10}$], $\text{Os}(\text{dppe})\text{Cp}^*$,^{11,12} $\text{MnI}(\text{dmpe})_2$,¹³ and $\text{W}(\text{dppe})_2$,¹⁴ in both homo- and heterobimetallic^{15–18} systems. Depending on the particular combination of metal and supporting ligands, a sequence of up to five interconvertible redox states ($n = 0, 1, 2, 3, \text{ or } 4$) has been observed in $[\{\text{L}_x\text{M}\}(\mu\text{-C}_4)\{\text{ML}_x\}]^{n+}$ systems,^{8,9,19} which can be further expanded by the introduction of redox-active supporting ligands.¹⁰ Carbon chains capped by bi-^{20,21} and polymetallic²² end-caps have been investigated in similar contexts, and redox-active oligomeric systems such as $[\text{Cl}(\text{depe})\text{Fe}\{\mu\text{-C}_4\}\{\text{dppe}\}_2\text{W}\{\mu\text{-C}_4\}\{\text{W}(\text{dppe})\}\{\mu\text{-C}_4\}\{\text{Fe}(\text{depe})_2\text{Cl}\}]^{23}$ and $[\{\text{Ru}_2(\mu\text{-ampy})_4\}\{\mu\text{-C}_4\}\{\text{Ru}_2(\mu\text{-ampy}')_4\}\{\mu\text{-C}_4\}\{\text{Ru}_2(\text{ampy})_4\}]$ ($\text{ampy}, \text{ampy}' = 2\text{-aminopyridines}$)²⁴ are also known.

$\text{ampy}, \text{ampy}' = 2\text{-aminopyridines}$)²⁴ are also known.

In all of the above examples, the π orbitals of the diyndiyl bridge mix with metal orbitals of appropriate symmetry to give occupied frontier orbitals that are more or less delocalized over both metal centers and the carbon bridge. Oxidation of these established examples of butadiyndiyl complexes results in removal of electrons from the largely delocalized frontier orbitals, giving rise to metal-stabilized tautomers of the C_4 chain from diyndiyl $[\{\text{L}_x\text{M}\}\text{-C}\equiv\text{C}-\text{C}\equiv\text{C}-\{\text{ML}_x\}]^{n+}$, through cumulene-like butatriene-bis-ylidene $[\{\text{L}_x\text{M}\}=\text{C}=\text{C}=\text{C}=\text{C}=\{\text{ML}_x\}]^{n+}$, to carbyne-like butyne-bis-triyl $[\{\text{L}_x\text{M}\}\equiv\text{C}-\text{C}\equiv\text{C}-\{\text{ML}_x\}]^{n+}$ forms; examples of metal complexes and clusters containing these various isomeric C_4 ligands have been isolated, and the most appropriate valence bond description of the $[\{\text{L}_x\text{M}\}(\mu\text{-C}_4)\{\text{ML}_x\}]$ moiety depends on the nature of the metal and the number of valence electrons.^{14,25–27} Many of the odd-electron radical cations $[\{\text{L}_x\text{M}\}(\mu\text{-C}_4)\{\text{ML}_x\}]^+$ have been described as class III “mixed valence” systems.²⁸ However, such

Received: August 1, 2011

Published: December 12, 2011

descriptions often lack the element of precision necessary to account for the contribution of the C_4 moiety to the stabilization of the unpaired electron. It would be better to more rigorously make the distinction between (i) genuinely delocalized mixed valence systems (class III), (ii) those that display fast electron exchange between the redox sites (class II–III), and (iii) systems in which the bridging ligand is so intimately involved in supporting the unpaired electron that the concept of redox noninnocent ligand behavior becomes a significant part of the overall description. Indeed, both experimental studies and theoretical calculations demonstrate that the electronic structure of complexes $[\{L_xM\}(\mu-C_4)\{ML_x\}]^{n+}$ can be fine-tuned by the identity of the metal end-cap, particularly with respect to the relative contributions of metal and carbon chain character to the frontier redox orbitals. For example, DFT calculations on the model systems $[\{M(dHpe)Cp\}_2(\mu-C_4)]^{n+}$ ($M = Fe$ or Ru ; $dHpe = H_2PCH_2CH_2PH_2$) reveal that the metal versus carbon chain character of the frontier molecular orbitals is directly dependent upon the identity of M , with the Fe derivatives more metal centered and conversely the Ru derivatives more heavily weighted on the carbon chain.¹⁷ As the proportion of metal:carbon chain character in these important frontier orbitals decreases, the complexes move between the extremes of redox-active metal fragments linked by a carbon chain and supporting genuine mixed valence concepts and examples of carbon fragments linking electron-donating metal fragments in which the bridging carbon chain can be thought of as redox noninnocent. This difference in the relative importance of the metal versus carbon chain character of the redox orbitals also becomes manifest in the structural and spectroscopic characteristics of the formally d^5/d^5 systems that approximate the descriptions of triplet $[\{L_xM\}-C\equiv C-C\equiv C-\{ML_x\}]^{n+}$ (most closely represented by $ML_x = Fe(dppe)Cp^*$, $n = 2$;⁵ $ML_x = Mn(dmpe)_2I$, $n = 0$;¹³) and singlet $[\{L_xM\}=C=C=C=C=\{ML_x\}]^{2+}$ (exemplified by $ML_x = Ru(PPh_3)_2Cp$,⁸ $Ru(dppe)Cp^*$,⁹ and $Re(PPh_3)(NO)Cp^*$.⁷

Although differences between the electronic structures of the $[\{L_xM\}(\mu-C_4)\{ML_x\}]^{n+}$ systems described above can be tracked back to fine details of the metal d/C_4 ligand π orbital overlap and occupancy, fundamentally the description of the metal to carbon chain interaction is very similar for the majority of pseudo-octahedral d^6 metal systems in which the σ_{M-C} bond is derived from overlap of the metal d_{z^2} and carbon ligand sp orbitals.^{7–19} The HOMO and HOMO–1 are approximately orthogonal and arise from efficient “in-plane” four-electron repulsive π -type interactions between metal and carbon chain fragment orbitals, and are illustrated in Figure 1 for the case of the computational model $\{M(dHpe)Cp\}_2(\mu-C\equiv C-C\equiv C)$ ($M = Fe, Ru$).

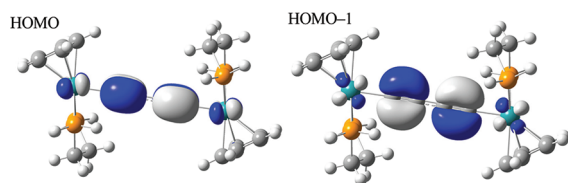


Figure 1. HOMO and HOMO–1 of $[\{Ru(dHpe)Cp\}_2(\mu-C\equiv C-C\equiv C)]$. HOMO composition: Ru_2 26%, C_4 62%; cf. $[\{Fe(dHpe)Cp\}_2(\mu-C\equiv C-C\equiv C)]$; Fe_2 41%, C_4 46%.

In this context, recent investigations on the cycloheptatrienyl molybdenum alkynyl complexes $[Mo(C\equiv CR)(dppe)(\eta-C_7H_7)]$ suggest the opportunity for a more fundamental control of the electronic structure of all-carbon-bridged bimetallic complexes by the metal end-cap.²⁹ As shown in Figure 2, although the bonding between the $Mo(dppe)(\eta-$

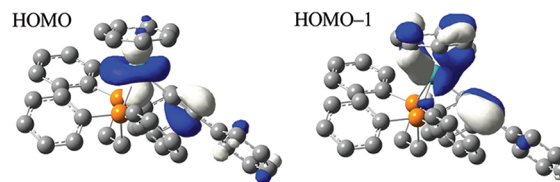


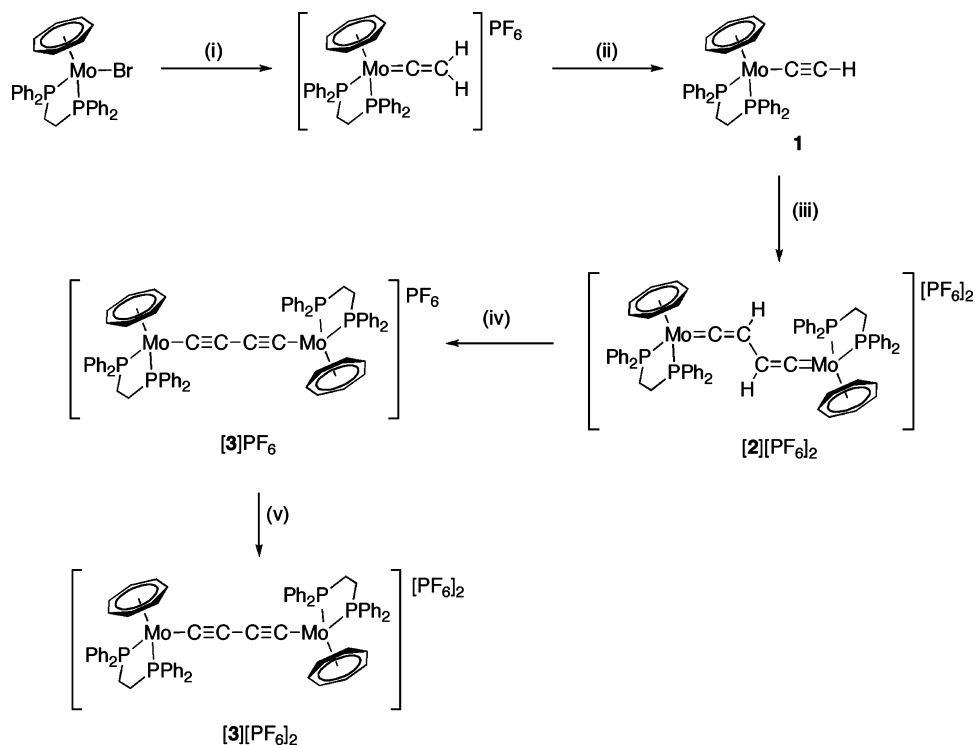
Figure 2. HOMO and HOMO–1 of $[Mo(C\equiv CPh)(dppe)(\eta-C_7H_7)]$ (B3LYP/SVP). Contour values of 0.04 au.²⁹

C_7H_7) unit and the alkynyl ligand also involves four-electron repulsive π -type interactions, critically, in the HOMO the overlap is between the $Mo d_{z^2}$ orbital and the carbon chain and is much less effective on symmetry grounds than the $d\pi-\pi$ interactions more commonly observed in half-sandwich d^6 complexes. This novel frontier orbital structure is often preserved upon oxidation and results in significant differences in the electronic and spectroscopic properties of $[Mo(C\equiv CR)(dppe)(\eta-C_7H_7)]^+$ systems when compared with analogous $[M(C\equiv CR)(dppe)Cp^*]^+$ ($M = Fe, Ru$) complexes. The d_{z^2} character in the HOMO of the cycloheptatrienyl derivatives can be attributed to the effects of strong metal–ring δ -bonding (evident in HOMO–1, Figure 2),^{30–32} which stabilize the $d\pi$ -type orbitals relative to those in cyclopentadienyl systems, and result in a significant modification in the d -orbital ordering.

In view of these observations, the introduction of the $Mo(dppe)(\eta-C_7H_7)$ end-cap into carbon-chain-bridged, bimetallic complexes may be expected to give rise to unusual electronic features as a consequence of the unique frontier orbital characteristics of the metal end-cap. In this work, we describe the synthesis, redox chemistry, and electronic structure of C_4 -bridged $[\{Mo(dppe)(\eta-C_7H_7)\}_2(\mu-C_4)]^{n+}$ ($n = 0, 1, \text{ or } 2$), which demonstrate a significant departure in properties from those generally attributed to the $[\{L_xM\}(\mu-C_4)\{ML_x\}]^{n+}$ class of complexes.

RESULTS AND DISCUSSION

Syntheses. The all-carbon-bridged complexes $[\{Mo(dppe)(\eta-C_7H_7)\}_2(\mu-C_4)]^{n+}$ ($n = 1, 2$) were prepared as outlined in Scheme 1, following a well-established route that has been utilized for the syntheses of the group 8 complexes $[\{M(dppe)Cp^*\}_2(\mu-C\equiv C-C\equiv C)]$ ($M = Fe^5$ or Ru^9), and isolated as the $[PF_6]^-$ salts. The pivotal step is the C_β -centered, radical–radical coupling of the 17-electron alkynyl complex $[Mo(C\equiv CH)(dppe)(\eta-C_7H_7)]^+$, leading to the construction of a four-carbon bridge in the form of a bis(vinylidene) complex, a process first proposed³³ to rationalize the formation of $[\{Fe(dppe)Cp^*\}_2(\mu-C=CMe-CMe=C)][BF_4]_2$ from oxidative coupling of $[Fe(C\equiv CHMe)(dppe)Cp^*][BF_4]$ and subsequently demonstrated for the cycloheptatrienyl molybdenum alkynyl radical $[Mo(C\equiv CPh)(dppe)(\eta-C_7H_7)]^+$ and a wide range of related alkynyl radicals.³⁴ The key precursor complex $[Mo(C\equiv CH)(dppe)(\eta-C_7H_7)]$, **1**, was prepared in stepwise fashion from $[MoBr(dppe)(\eta-C_7H_7)]$ by initial conversion to the vinylidene $[Mo(C=CH_2)(dppe)(\eta-C_7H_7)]^+$, through reaction with $HC\equiv CSiMe_3$, and subsequent

Scheme 1^a

^aReagents and conditions: (i) $\text{HC}\equiv\text{CSiMe}_3/\text{KPF}_6$ in MeOH, reflux 3 h. (ii) Excess KOBu^t in thf, 1 h. (iii) $[\text{FeCp}_2]\text{PF}_6$ in thf (-78°C), 5 h. (iv) KOBu^t in thf, 5 h, aerial oxidation. (v) $[\text{FeCp}_2]\text{PF}_6$ in CH_2Cl_2 , 1 h.

Table 1. Electrochemical Data for $[\{\text{L}_x\text{M}\}(\mu\text{-C}_4)\{\text{ML}_x\}]^{n+\alpha}$

ML_x	E_1	E_2	E_3	E_4	$E_2 - E_1$	$K_C(+1/+2)$	ref
$\text{Mo}(\text{dppe})(\eta\text{-C}_7\text{H}_7)^b$	-1.02	-0.59	0.39	0.48	0.43	1.9×10^7	this work
$\text{Fe}(\text{dppe})\text{Cp}^*$	-1.14	-0.42	0.49		0.72	1.6×10^{12}	5, 6
$\text{Ru}(\text{dppe})\text{Cp}^*$	-0.89	-0.24	0.58	1.05	0.65	9.7×10^{10}	9
$\text{Os}(\text{dppe})\text{Cp}^*$	-1.08	-0.47	0.36	0.80	0.61	2.1×10^{10}	11
$\text{Re}(\text{NO})(\text{PPh}_3)\text{Cp}^*$	-0.45	0.08			0.53	1.1×10^9	7

^aAll potentials are reported with reference to the $\text{FeCp}_2/[\text{FeCp}_2]^+$ couple ($E_{1/2} = 0.00\text{ V}$). Data from literature sources are adjusted via $E_{1/2}$ cited for the $\text{FeCp}_2/[\text{FeCp}_2]^+$ couple (0.46 V vs SCE in 0.1 M $[\text{Bu}_4^{\text{n}}\text{N}]\text{PF}_6/\text{CH}_2\text{Cl}_2$ solution at a Pt electrode). ^bCyclic voltammogram recorded ($\nu = 100\text{ mV s}^{-1}$) from a 0.2 M $[\text{Bu}_4^{\text{n}}\text{N}]\text{PF}_6/\text{CH}_2\text{Cl}_2$ solution at a glassy carbon working electrode.

deprotonation with a 10-fold excess of KOBu^t in thf; similar protocols have been employed elsewhere.^{5,9,35} The requirement for a large excess of base to shift the vinylidene/alkynyl equilibrium to the alkynyl form may arise from a combination of the very strong electron donor properties of the $\text{Mo}(\text{dppe})(\eta\text{-C}_7\text{H}_7)$ unit, rendering the vinylidene $[\text{Mo}(\text{C}=\text{CH}_2)(\text{dppe})(\eta\text{-C}_7\text{H}_7)]\text{PF}_6$ a relatively weak acid and the strong $\text{Mo}=\text{C}_\alpha$ bond of the group 6 vinylidene complexes.^{36,37} The identity of complex **1** was confirmed by spectroscopic data, which include a strong IR-active $\nu(\text{C}\equiv\text{C})$ stretch at 1908 cm^{-1} typical of unsubstituted alkynyl complexes $[\{\text{L}_x\text{M}\}-\text{C}\equiv\text{CH}]$,^{5,9} a triplet $\{J(\text{P}-\text{H}) = 4\text{ Hz}\}$ at δ_{H} 1.74 assigned to the alkynyl H substituent, a triplet $\{J(\text{P}-\text{C}) = 25\text{ Hz}\}$ at δ_{C} 130.1 assigned to the alkynyl C_α carbon, and microanalytical data.

The cyclic voltammogram of complex **1** in thf/0.1 M $[\text{Bu}_4^{\text{n}}\text{N}]\text{PF}_6$ exhibited an irreversible oxidation at ambient temperatures, but on cooling to -40°C , a chemically reversible process ($E_{1/2} = -0.70\text{ V}$ vs $\text{FeCp}_2/[\text{FeCp}_2]^+$) was observed. Therefore to ensure the accumulation of the 17-electron radical $[\text{Mo}(\text{C}\equiv\text{CH})(\text{dppe})(\eta\text{-C}_7\text{H}_7)]^+$, **1**⁺, in solution necessary to promote efficiently the coupling reaction outlined in Scheme 1,

the reaction of **1** with $[\text{FeCp}_2]\text{PF}_6$ was conducted at low temperature (-78°C) as a concentrated solution in thf. After 5 h a deep purple solid containing the required product, $[\{\text{Mo}(\text{dppe})(\eta\text{-C}_7\text{H}_7)\}_2(\mu\text{-C}=\text{CH}-\text{CH}=\text{C})][\text{PF}_6]_2$, **2** $[\text{PF}_6]_2$, as a mixture with $[\text{Mo}(\text{C}=\text{CH}_2)(\text{dppe})(\eta\text{-C}_7\text{H}_7)]\text{PF}_6$,³⁶ was obtained, the components being separable by recrystallization given the lower solubility of **2** $[\text{PF}_6]_2$. The unavoidable formation of small quantities of $[\text{Mo}(\text{C}=\text{CH}_2)(\text{dppe})(\eta\text{-C}_7\text{H}_7)]\text{PF}_6$, evident from NMR monitoring of the crude reaction mixture (approximate ratio in a typical preparation $[\text{Mo}(\text{C}=\text{CH}_2)(\text{dppe})(\eta\text{-C}_7\text{H}_7)]\text{PF}_6:\mathbf{2}[\text{PF}_6]_2 = 1:4$), probably results from abstraction of H^\bullet from the solvent by the reactive radical **1**⁺; an identical, albeit much slower, process has been suggested for the more sterically congested radical $[\text{Mo}(\text{C}\equiv\text{C}\text{Bu}^t)(\text{dppe})(\eta\text{-C}_7\text{H}_7)]^+$.^{34a} The low-field $\text{Mo}=\text{C}_\alpha$ resonance of **2** $[\text{PF}_6]_2$ was not detected in the $^{13}\text{C}\{^1\text{H}\}$ NMR spectrum, but a triplet resonance at δ 4.41, characteristic of a vinylidene proton was observed in the ^1H NMR spectrum.

The deprotonation of complex **2** $[\text{PF}_6]_2$ was effected with excess KOBu^t in thf at room temperature to give a green-brown

solution, from which $[\{\text{Mo}(\text{dppe})(\eta\text{-C}_7\text{H}_7)\}_2(\mu\text{-C}_4)]\text{PF}_6$, $[\mathbf{3}]\text{PF}_6$, was isolated as a green-brown solid together with small quantities of neutral, orange-brown $[\{\text{Mo}(\text{dppe})(\eta\text{-C}_7\text{H}_7)\}_2(\mu\text{-C}\equiv\text{C}\equiv\text{C})]$, $\mathbf{3}$. The isolation of the oxidized species $[\mathbf{3}]\text{PF}_6$ as the major product from the deprotonation reaction contrasts with the corresponding reactions of $[\{\text{M}(\text{dppe})\text{Cp}^*\}_2(\mu\text{-C}=\text{CH}-\text{CH}=\text{C})]^{2+}$ ($\text{M} = \text{Fe}$ or Ru), which lead to formation of the neutral diyndiyl complexes $[\{\text{M}(\text{dppe})\text{Cp}^*\}_2(\mu\text{-C}\equiv\text{C}-\text{C}\equiv\text{C})]$, but is consistent with related facile oxidation chemistry of the $\text{Mo}(\text{dppe})(\eta\text{-C}_7\text{H}_7)$ auxiliary.³⁸ Complexes $\mathbf{3}$ and $[\mathbf{3}]\text{PF}_6$ were identified by mass spectrometry and microanalytical data (see Experimental Section) and further characterized by a series of techniques including cyclic voltammetry, IR, NIR, and Raman spectroscopy as detailed below.

Electrochemistry and Synthetic Redox Chemistry.

The cyclic voltammogram of $[\mathbf{3}]\text{PF}_6$ was recorded at a glassy carbon electrode in $\text{CH}_2\text{Cl}_2/0.2 \text{ M } [\text{Bu}_4^{\text{n}}\text{N}]\text{PF}_6$; a summary of $E_{1/2}$ data for $[\mathbf{3}]\text{PF}_6$, relative to the $\text{FeCp}_2/[\text{FeCp}_2]^+$ couple, and a comparison with selected, closely related systems from groups 7 and 8 are presented in Table 1.

The cyclic voltammogram of $[\mathbf{3}]\text{PF}_6$ exhibits four redox processes. The well-separated waves at lowest potential $E_1 = -1.02 \text{ V}$, $E_2 = -0.59 \text{ V}$ are assigned to the couples $\mathbf{3}/[\mathbf{3}]^+$ and $[\mathbf{3}]^+ / [\mathbf{3}]^{2+}$ on the basis of comparison with the related diyndiyl complexes in Table 1 and the redox potential for the monometallic diyndyl complex $[\text{Mo}(\text{C}\equiv\text{C}-\text{C}\equiv\text{CH})(\text{dppe})(\eta\text{-C}_7\text{H}_7)]$ ($E_{1/2} = -0.58 \text{ V}$ in CH_2Cl_2 vs $\text{FeCp}_2/[\text{FeCp}_2]^+$).³⁹ These first two waves are fully chemically and electrochemically reversible [$i_p^{\text{C}}/i_p^{\text{A}} = 1$ and $i_p \propto \nu^{1/2}$], and the relatively small difference in the first and second oxidation potentials in the molybdenum complex ($E_2 - E_1 = 0.43 \text{ V}$) also leads to the smallest K_C value in the series (see Table 1). The more negative value of $E_{1/2}$ for the couple $\mathbf{3}/[\mathbf{3}]^+$ by comparison with $[\text{Mo}(\text{C}\equiv\text{C}-\text{C}\equiv\text{CH})(\text{dppe})(\eta\text{-C}_7\text{H}_7)]^{0/+}$ is consistent with a degree of synergy between the two electron-donating $\text{Mo}(\text{dppe})(\eta\text{-C}_7\text{H}_7)$ fragments. However, although in monometallic systems of the type $[\text{M}\{\text{C}\equiv\text{C}\}_n\text{R}\{\text{dppe})(\eta\text{-L})]$ ($\eta\text{-L} = \eta\text{-C}_5\text{Me}_5 = \text{Cp}^*$, $\text{M} = \text{Fe}$,^{18,40} or Ru ;^{41,42} $\eta\text{-L} = \eta\text{-C}_7\text{H}_7$, $\text{M} = \text{Mo}$,^{29,39}), the $E_{1/2}$ value for one-electron oxidation is always the most negative for the $\text{Mo}(\text{dppe})(\eta\text{-C}_7\text{H}_7)$ system,⁴³ this is not so for the bimetallic diyndiyl complexes, where the iron complex $[\{\text{Fe}(\text{dppe})\text{Cp}^*\}_2(\mu\text{-C}\equiv\text{C}\equiv\text{C})]$ is the most easily oxidized (in the thermodynamic sense) member of the family (Table 1). In common with $[\{\text{M}(\text{dppe})\text{Cp}^*\}_2(\mu\text{-C}\equiv\text{C}\equiv\text{C})]$ ($\text{M} = \text{Ru}$ or Os), two further redox processes are observed for the $\text{Mo}(\text{dppe})(\eta\text{-C}_7\text{H}_7)$ system, viz., $E_3 = 0.39 \text{ V}$, $E_4 = 0.48 \text{ V}$ assigned to the couples $[\mathbf{3}]^{2+}/[\mathbf{3}]^{3+}$ and $[\mathbf{3}]^{3+}/[\mathbf{3}]^{4+}$. These waves are very closely spaced, and therefore the degree of reversibility is much harder to assess, although no redox-active secondary products were observed in the potential range investigated. We note that the relatively electron rich system $[\{\text{Fe}(\text{dppe})\text{Cp}^*\}_2(\mu\text{-C}\equiv\text{C}\equiv\text{C})]$ undergoes three chemically reversible redox processes, the first two of which are principally metal in character and the third being more closely associated with oxidation of the carbon chain.⁶

Guided by the electrochemical results, synthetic studies were carried out to generate the dication $[\{\text{Mo}(\text{dppe})(\eta\text{-C}_7\text{H}_7)\}_2(\mu\text{-C}_4)]^{2+}$, $[\mathbf{3}]^{2+}$, using chemical redox reagents. Reaction of a solution of green-brown $[\mathbf{3}]\text{PF}_6$ with an excess of $[\text{FeCp}_2]\text{PF}_6$ in CH_2Cl_2 resulted in the formation of an intense green solution, from which $[\{\text{Mo}(\text{dppe})(\eta\text{-C}_7\text{H}_7)\}_2(\mu\text{-C}_4)][\text{PF}_6]_2$, $[\mathbf{3}][\text{PF}_6]_2$, was isolated as a deep green solid (Scheme 1).

Complex $[\mathbf{3}][\text{PF}_6]_2$ (which exhibits identical electrochemical behavior to that of $[\mathbf{3}]\text{PF}_6$) was characterized by a series of spectroscopic and spectroelectrochemical techniques (see below), and its identity further confirmed by a single-crystal X-ray structural investigation.

Structural Investigations. The molecular structure of $[\{\text{Mo}(\text{dppe})(\eta\text{-C}_7\text{H}_7)\}_2(\mu\text{-C}_4)][\text{PF}_6]_2$, $[\mathbf{3}][\text{PF}_6]_2$, is shown in Figure 3, and important bond lengths and angles are

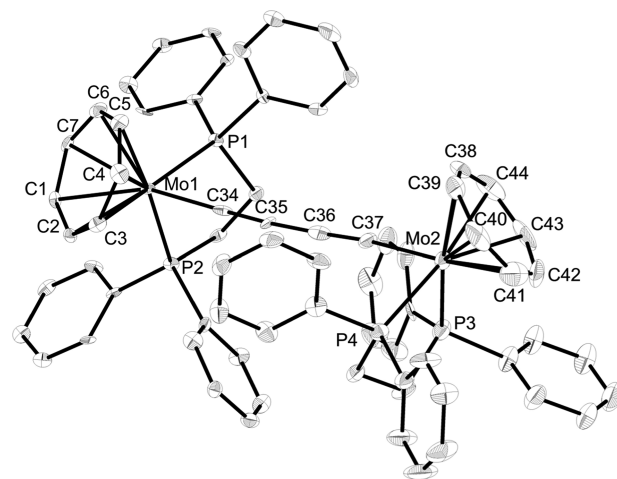


Figure 3. Molecular structure of $[\mathbf{3}][\text{PF}_6]_2$ with thermal ellipsoids plotted at 50% probability. $[\text{PF}_6]^-$ counterions, solvent of crystallization, and H atoms are removed for clarity.

summarized in Table 2, while Table 3 presents some key comparisons with closely related all-carbon-bridged complexes.

Table 2. Important Bond Lengths (Å) and Angles (deg) for Complex $[\mathbf{3}][\text{PF}_6]_2$

Mo(1)–C(34)	2.041(7)	Mo(1)–C(34)–C(35)	177.0(7)
Mo(2)–C(37)	2.024(7)	C(34)–C(35)–C(36)	176.4(7)
C(34)–C(35)	1.211(9)	C(35)–C(36)–C(37)	177.5(8)
C(35)–C(36)	1.355(9)	C(36)–C(37)–Mo(2)	174.1(6)
C(36)–C(37)	1.249(9)	P(1)–Mo(1)–P(2)	79.26(6)
Mo(1)–P(1)	2.5070(19)	P(1)–Mo(1)–C(34)	75.1(2)
Mo(1)–P(2)	2.5238(17)	P(2)–Mo(1)–C(34)	81.04(18)
Mo(2)–P(3)	2.526(2)	P(3)–Mo(2)–P(4)	79.99(7)
Mo(2)–P(4)	2.539(2)	P(3)–Mo(2)–C(37)	84.0(2)
		P(4)–Mo(2)–C(37)	75.0(2)

The presence of a four-carbon bridge, $\text{C}(34)\text{--}\text{C}(35)\text{--}\text{C}(36)\text{--}\text{C}(37)$, linking the $\text{Mo}(\text{dppe})(\eta\text{-C}_7\text{H}_7)$ end-caps is confirmed by the structural study. The two $\text{Mo}(\text{dppe})(\eta\text{-C}_7\text{H}_7)$ units are disposed in a *gauche* arrangement with the angle between planes defined by $\text{Ct}(1)\text{--}\text{Mo}(1)\text{--}\text{C}(34)$ and $\text{Ct}(2)\text{--}\text{Mo}(2)\text{--}\text{C}(37)$ [$\text{Ct}(1)$, $\text{Ct}(2)$ are the centroids of the C_7H_7 rings attached to $\text{Mo}(1)$ and $\text{Mo}(2)$] calculated as 80.8° . As discussed, the redox behavior of diyndiyl-bridged bimetallic complexes falls into two broad classes represented by the contrasting properties of those systems that feature predominantly metal-based redox chemistry, such as $[\{\text{Fe}(\text{dppe})\text{Cp}^*\}_2(\mu\text{-C}_4)]^{n+}$ ⁵ and $[\{\text{MnI}(\text{dmppe})_2\}(\mu\text{-C}_4)]^{n+}$,¹³ and those systems in which the C_4 ligand is more intimately involved in the redox events, such as $[\{\text{Ru}(\text{dppe})\text{Cp}^*\}_2(\mu\text{-C}_4)]^{n+}$ ⁹ and $[\{\text{Re}(\text{PPh}_3)(\text{NO})\text{Cp}^*\}_2(\mu\text{-C}_4)]^{n+}$.⁷ The structural differences between the two classes are manifest in the changes in carbon–

Table 3. Bond Length Parameters (Å) for Selected $[\{ML_x\}\{\mu-C(\alpha)\equiv C(\beta)-C(\beta')\equiv C(\alpha')\}\{ML_x\}]^{n+}$ Complexes

ML_x	n	$C(\alpha)-C(\beta)$, $C(\alpha')-C(\beta')$	$C(\beta)-C(\beta')$	$M-C(\alpha)$, $M-C(\alpha')$	ref
Ru(dppe) Cp*	0	1.223(4), 1.218(4)	1.382(4)	2.001(3), 2.003(3)	9
Ru(dppe) Cp*	1	1.248(3)	1.338(3)	1.931(2)	9
Ru(dppe) Cp*	2	1.280(7), 1.269(7)	1.294(7)	1.858(5), 1.856(5)	9
Re(PPh ₃) (NO)Cp*	0	1.202(7)	1.389(5)	2.037(5)	7
Re(PPh ₃) (NO)Cp*	2	1.263(10), 1.260(10)	1.305(10)	1.909(7), 1.916(7)	7
Fe(dppe) Cp*	0	1.220(4), 1.221(4)	1.373(4)	1.889(3), 1.884(3)	16
Fe(dppe) Cp*	1	1.236(9)	1.36(1)	1.830(8)	5
Mo(dppe)(η - C ₇ H ₇)	2	1.211(9), 1.249(9)	1.355(9)	2.041(7), 2.024(7)	this work

carbon bond lengths along the C₄ chain as a function of redox state. In the case of the Ru and Re complexes for which the redox events involve significant carbon chain character, proceeding from $n = 0$ to $n = +2$, there is a distinct elongation of C(α)–C(β), and C(α')–C(β') and corresponding shortening of the central C(β)–C(β') bond, consistent with the evolution of a cumulenic structure in the dication.⁹ By contrast, in the iron system, the first two redox processes have substantial metal character, and this is reflected in the much smaller changes in the geometry of the carbon chain (although structural data for the dication are not available);^{5,16} the third redox event is probably more carbon-centered.^{6,16} Inspection of the data in Table 3 suggests that the carbon chain in the dication [3][PF₆]₂ retains a degree of alternating triple/single-bond character. Moreover the Mo–C(α) bond distances in [3][PF₆]₂ (2.041(7), 2.024(7) Å), although probably shorter than that determined for the alkynyl radical cation [Mo(C≡CPh)(dppe)(η -C₇H₇)] [BF₄], 2.067(9) Å,⁴⁴ are longer than the equivalent parameter in the closely related bis(vinylidene)-bridged [$\{Mo(dppe)(\eta-C_7H_7)\}_2(\mu-C=CPh-CPh=C)\]$ [PF₆]₂ (1.951(5) Å).³⁶ By comparison, the Ru–C(α) bond lengths of 1.858(5) and 1.856(5) Å, reported for [$\{Ru(dppe)Cp^*\}_2(\mu-C_4)\]^{2+}$, are only marginally longer than Ru–C(α) distances in the bis(vinylidene)-bridged analogue [$\{Ru(dppe)Cp^*\}_2(\mu-C=CH-CH=C)\]$ [PF₆]₂ (1.837(4), 1.834(4) Å). The key bond length parameters along the carbon chain in [3][PF₆]₂ are therefore not typical of the cumulenic [$\{L_xM\}=C=C=C=C=\{ML_x\}\]^{2+}$ structure normally exhibited by formally d⁵/d⁵ systems of 4d and 5d series metals.

Vibrational Spectroscopy. The response of the $\nu(C\equiv C)$ modes of the $\mu-C_4$ bridging ligand in [$\{L_xM\}(\mu-C_4)\{ML_x\}\]^{n+}$ to changes in charge state, n , is a useful probe of the extent of involvement of the carbon chain bridge in the redox orbitals.^{5,7,9,13} Therefore, in the current work, the characteristics of the $\nu(C\equiv C)$ modes of 3, [3]PF₆, and [3][PF₆]₂ are of specific importance and were investigated by a combination of IR and Raman spectroscopy on isolated samples, complemented by an IR spectroelectrochemical study. Starting from [3]PF₆, the spectroelectrochemical generation of 3 and [3][PF₆]₂ was fully reversible with complete recovery of the spectrum of [3]PF₆. However, despite the apparent reversibility of the electrochemical events on the time scale of cyclic voltammetry, attempts at further oxidation to [3][PF₆]₃ and [3][PF₆]₄ resulted only in decomposition in the room-

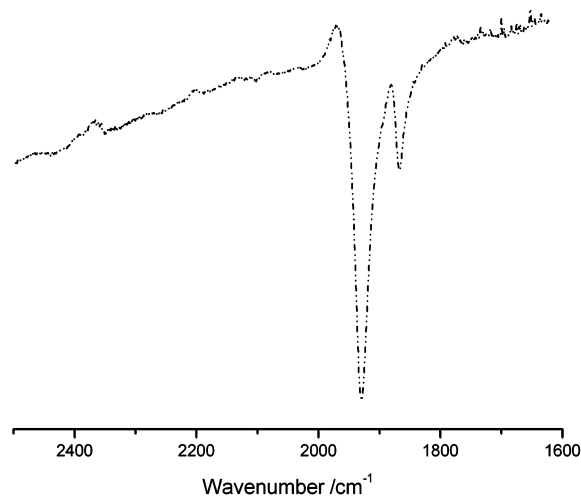
temperature spectroelectrochemical cell. A summary of the IR and Raman data obtained for [3]^{*n*+} ($n = 0, 1$, or 2) is presented in Table 4 alongside comparative data for [$\{Re(PPh_3)(NO)-Cp^*\}_2(\mu-C_4)\]^{n+}$ ($n = 0, 1$, or 2).⁷

Table 4. Infrared and Raman Data (cm⁻¹) for $\nu(C\equiv C)$ Stretching Modes of the C₄ Bridge of [$\{L_xM\}(\mu-C_4)\{ML_x\}\]^{n+}$

ML_x	$n = 0$		$n = 1$		$n = 2$	
	IR	Raman	IR	Raman	IR	Raman
Mo(dppe)(η - C ₇ H ₇)	not obsd	1939	1930, 1868	1800	not obsd	1894, 1826
Re(PPh ₃) (NO)Cp*	1964	2056	1872	1990	not obsd	1883

^aIR data in CH₂Cl₂ solution; not obsd = not observed. Raman spectra for [3]^{*n*+} recorded in the solid state ($\lambda_{ex} = 532.2$ nm).

The neutral diyndiyl complex 3 is IR silent in the region 2500–1550 cm⁻¹, but a Raman band is observed from a solid sample at 1939 cm⁻¹ ($\lambda_{ex} = 532.2$ nm); each of these observations is consistent with a symmetrical electronic structure. By contrast, [3]PF₆ exhibits a distinctive, intense two-band IR spectrum in CH₂Cl₂ solution with $\nu(C\equiv C)$ 1930, 1868 cm⁻¹ (Figure 4); the tail of a relatively intense NIR

**Figure 4.** IR spectrum of [3]PF₆ in CH₂Cl₂.

absorption band is also apparent in Figure 4 intruding into the IR region (see later). In the solid-state Raman spectrum of [3]PF₆, a band at 1800 cm⁻¹ was detected arising from a symmetric $\nu(C\equiv C)$ mode. While the observation of two IR-active $\nu(C\equiv C)$ modes for the mixed valence monocation [3]PF₆ may arise from the presence of different conformers, associated with the relative dispositions of the two metal end-caps,⁴⁵ the relative intensities of the two IR-active $\nu(C\equiv C)$ modes of [3]PF₆ did not alter significantly with change in solvent polarity or in the solid state. Moreover, typical homobimetallic, C₄-bridged complexes of the 4d/5d metals [$\{ML_x\}_2(\mu-C_4)\]^{n+}$ ($ML_x = Ru(dppe)Cp^*$, $Re(NO)(PPh_3)-Cp^*$)^{7,9} exhibit only a single IR-active $\nu(C\equiv C)$ mode in the mixed valence state. An alternative rationalization for the IR spectral properties of [3]PF₆, consistent with the results of NIR and EPR spectroscopy (see below), is the adoption of a localized electronic structure resulting from slow intervalence

electron transfer on the IR time scale. For the dication $[3][PF_6]_2$, no IR-active bands were observed for an isolated sample in solution in CH_2Cl_2 ; however the Raman spectrum of $[3][PF_6]_2$ as a solid sample featured two bands at 1826 and 1894 cm^{-1} . A single strong band in this region would be expected for a symmetric $[\{L_xM\}=C=C=C=C=\{ML_x\}]^{2+}$ structure, but the observation of two bands may be due to the presence of different conformations of $[3]^{2+}$ in the solid state or possibly indicative of a Raman-active impurity. Raman spectra of solid $[3][PF_6]_2$ collected using different excitation wavelengths (532.2, 632.8, 785.1 nm) reveal that these bands are enhanced to different extents, supporting the notion that the two bands arise from two different forms of the species, or two chemically distinct species, in the sample. However, the absence of an IR-active $\nu(C\equiv C)$ band in $[3][PF_6]_2$ requires any putative impurity to have a high-symmetry structure. Interpretation of the trend in the Raman-active $\nu(C\equiv C)$ frequency along the series $[3]^{n+}$ ($n = 0, 1, \text{ or } 2$) (see Table 4) is not straightforward. However, the sequential shift of $\nu(C\equiv C)$ to lower wavenumber, observed in the Raman data for $[\{Re(PPh_3)(NO)Cp^*\}_2(\mu-C_4)]^{n+}$ and indicative of the progressive evolution of cumulenic character to the all-carbon bridge with increasing n , appears not to be a feature of $[3]^{n+}$.

Electronic Spectroscopy. The UV-vis-NIR spectra of $[3]^{n+}$ ($n = 0, 1, \text{ or } 2$) collected by spectroelectrochemical methods are presented in Figure 5. The interconversion

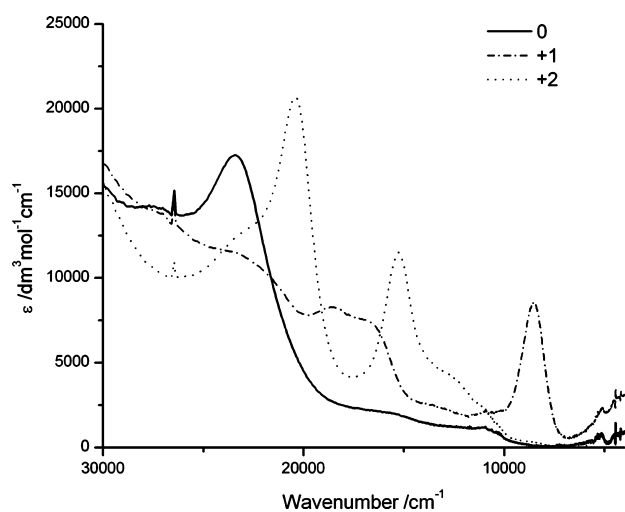


Figure 5. Spectroelectrochemically generated UV-vis-NIR spectra of **3** (solid line), $[3]^+$ (broken line), and $[3]^{2+}$ (dotted line) in $CH_2Cl_2/0.1 M [Bu_4N]PF_6$.

between these redox states was fully reversible with recovery of spectra on stepwise oxidation or reduction.

The UV-vis-NIR spectrum of **3** is dominated by an absorption at 23 600 $cm^{-1}/423 \text{ nm}$ ($\epsilon 17\,100 \text{ M}^{-1} \text{ cm}^{-1}$), which was assigned (with reference to the spectrum of $[Mo(C\equiv CPh)(dppe)(\eta-C_7H_7)]^{29}$ to transitions from the metal (or mixed metal and carbon chain) to π^* acceptor orbitals on the C_4 ligand, which may be denoted as a mixed MLCT/ILCT transition. Similar transitions, albeit less well resolved, can also be observed in the spectrum of $[Mo(C\equiv C\equiv CSiMe_3)(dppe)(\eta-C_7H_7)]^{46}$. In the dication $[3][PF_6]_2$, the principal absorptions of interest are at 20 500 $cm^{-1}/487 \text{ nm}$ ($\epsilon 20\,500 \text{ M}^{-1} \text{ cm}^{-1}$) and 15 300 $cm^{-1}/653 \text{ nm}$ ($\epsilon 11\,300 \text{ M}^{-1} \text{ cm}^{-1}$). These bands are similar in structure to absorptions

observed in the range 18 000–16 000 cm^{-1} for the related monometallic radical cations^{29,46} $[Mo(C\equiv CPh)(dppe)(\eta-C_7H_7)]^+$ and $[Mo(C\equiv C-C\equiv CSiMe_3)(dppe)(\eta-C_7H_7)]^+$, which were assigned to LMCT transitions from the carbon chain to the formally oxidized $Mo(dppe)(\eta-C_7H_7)$ unit. While similar bands can be observed, albeit with less resolution, in the UV-vis spectrum of $[3]^+$, the most significant spectroscopic features of the monocation are found in the NIR region of the spectrum. Two band envelopes are evident in the NIR spectrum, a relatively sharp absorption at 8650 cm^{-1} ($\epsilon 8300 \text{ M}^{-1} \text{ cm}^{-1}$) and a much broader feature centered at 4020 cm^{-1} ($\epsilon 2900 \text{ M}^{-1} \text{ cm}^{-1}$), which tails into the IR region (see Figures 4, 5, and 6).

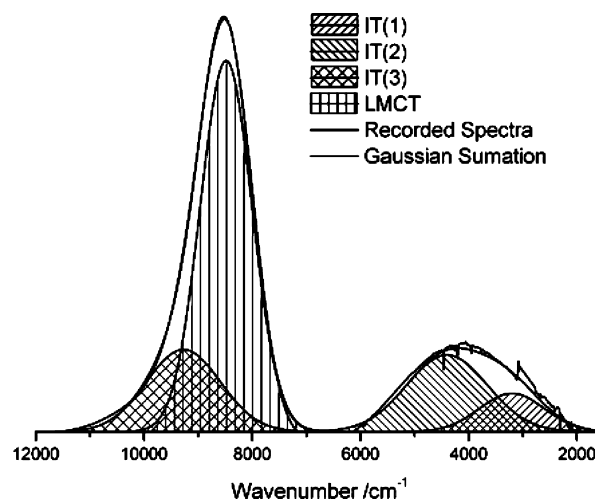


Figure 6. Near-IR-IR region of $[3]PF_6$ in CH_2Cl_2 , showing the deconvolution into the sum of four Gaussian-shaped absorption bands.

To assist in the interpretation of the NIR data, spectra of isolated samples of $[3]PF_6$ were collected in a range of solvents and spectral deconvolution in the region 12 000 to 2000 cm^{-1} was carried out (Figure 6 and Table 5).

Deconvolution of the spectrum recorded in CH_2Cl_2 reveals a total of four Gaussian-shaped absorption bands centered at 3200 cm^{-1} , IT(1); 4400 cm^{-1} , IT(2); 8500 cm^{-1} , LMCT; and 9300 cm^{-1} , IT(3). The form of the spectrum is sensitive to solvent polarity, and therefore the deconvolution procedure was repeated for spectra obtained in MeCN and acetone; results are summarized in Table 5. The bands labeled IT(1), IT(2), and IT(3) exhibit strong solvatochromic dependence; for example IT(2) shifts to high energy by approximately 1500 cm^{-1} between CH_2Cl_2 and acetone. By contrast, the more intense band at 8500 cm^{-1} was relatively insensitive to solvent variation with a shift not exceeding 300 cm^{-1} . The interpretation and assignment of the NIR region of the spectrum of mixed valence complexes presents a significant challenge especially in systems featuring heavier transition metals, due to multiple absorptions arising from the non-degenerate character of the metal d orbitals.^{47,48} Assuming a description of the electronic transitions in terms of metal-localized oxidation events, the three lower intensity, solvent-sensitive NIR transitions observed for $[3]PF_6$ [IT(1), IT(2), and IT(3)] can be assigned to three out of the five possible transitions comprising three intervalence charge transfer (IVCT) (or MMCT, metal-metal charge transfer) bands and two interconfigurational (or metal-localized dd) transitions.⁴⁷

Table 5. Analysis of the NIR Region of the Spectrum of [3]PF₆

band	CH ₂ Cl ₂			MeCN			acetone		
	ν/cm^{-1}	$\Delta\nu_{1/2}/\text{cm}^{-1}$	$\epsilon/\text{M}^{-1}\text{cm}^{-1}$	ν/cm^{-1}	$\Delta\nu_{1/2}/\text{cm}^{-1}$	A^a	ν/cm^{-1}	$\Delta\nu_{1/2}/\text{cm}^{-1}$	A^a
IT(1)	3200	1200	870	3500	1600	0.04	3900	2000	0.06
IT(2)	4400	1500	1750	5300	1900	0.04	5900	2000	0.05
IT(3)	9300	1370	1750	10 100	1400	0.04	10 250	1400	0.04
LMCT	8500	900	8440	8750	1100	0.17	8650	1200	0.21

^aA = absorbance. Samples of [3]PF₆ were not fully soluble in MeCN or acetone, and therefore accurate concentrations and extinction coefficients could not be obtained in these solvents.

Given the low intensity of dd bands associated with [Mo(C≡CR)(dppe)(η-C₇H₇)]⁺ (R = aryl) cations,²⁹ transitions IT(1), IT(2), and IT(3) are assigned to IVCT processes. The remaining band at 8500 cm⁻¹ is distinct in terms of the small $\Delta\nu_{1/2}$ parameter, relatively high extinction coefficient, and limited solvatochromic dependence (Figure 6, Table 5) and is therefore provisionally assigned to a LMCT process.

The low-energy and relatively small extinction coefficients (ca. 10³ M⁻¹ cm⁻¹) of absorptions IT(1), IT(2), and IT(3) in [3]PF₆ are similar to IVCT bands in the heterobimetallic complexes [Fe(dppe)Cp*](μ-C₄){ML_x}⁺ (ML_x = Re(NO)(PPh₃)Cp* or Ru(dppe)Cp*),^{15,17} indicative of rather weak electronic coupling in [3]PF₆. However further analysis of bands IT(1), IT(2), and IT(3) reveals that the band widths are narrower than predicted from the two-state model of Hush.^{28b,49} For example, for band IT(1) in CH₂Cl₂, the experimental $\Delta\nu_{1/2}$ parameter (1200 cm⁻¹) is significantly narrower than the calculated Hush value (2720 cm⁻¹).⁵⁰ IVCT bands that are narrower than calculated from the Hush model indicate deviations from the localized two-state model and are often interpreted in terms of electronically delocalized class III behavior. However, for [3]PF₆ the NIR band envelopes of the three IVCT bands exhibit pronounced solvatochromic shifts, consistent with an assignment of these transitions as charge transfer bands and necessitating a description of [3]PF₆ in terms of localized oxidation states, which is also in keeping with the IR and Raman data. The deviations in band shape from the predictions of the two-state model are therefore attributed to involvement of the bridging ligand in the charge transfer process, which has been shown elsewhere to result in significant narrowing of the band shape.^{49,51}

EPR Spectroscopy and Magnetochemistry. The characterization of [L_xM](μ-C₄){ML_x}⁺ by EPR spectroscopy can in principle provide information on both the location of the unpaired electron and the rate of electron transfer in formally mixed valence systems, especially when used in concert with other spectroscopic methods.^{7,15} For example, in the rhenium complex [Re(NO)(PPh₃)Cp*]₂(μ-C₄)⁺, it was possible to resolve the hyperfine coupling arising from two rhenium centers (*I* = 5/2), rendered equivalent by electron transfer between the two metal end-caps at a rate faster than the EPR time scale. Moreover *A*_{iso}(Re) values were one-half of those observed for typical related monometallic radicals, indicating full delocalization of the odd electron between the two Re centers on the time scale of X-band EPR spectroscopy.⁷ Conversely, the broad EPR signal for [W(dppe)₂](μ-C₄)⁺, observed only at temperatures below 160 K, is consistent with electron transfer between the tungsten end-caps at a rate comparable with the EPR time scale.¹⁴

Monometallic carbon chain radicals of the type [Mo{(C≡C)_nR}(dppe)(η-C₇H₇)]⁺ (*n* = 1 or 2; R = H, aryl, SiMe₃) exhibit X-band EPR solution spectra with well-resolved

hyperfine couplings to ^{95/97}Mo, ³¹P, and ¹H(C₇H₇).^{29,46,52} and therefore the application of this technique to [3]⁺ and [3]²⁺ may provide useful data on the location of unpaired spin density in these systems. The X-band, CH₂Cl₂ solution EPR spectrum of the monocation [3]PF₆, recorded at 243 K, is shown in Figure 7. With the exception of the broad shoulder

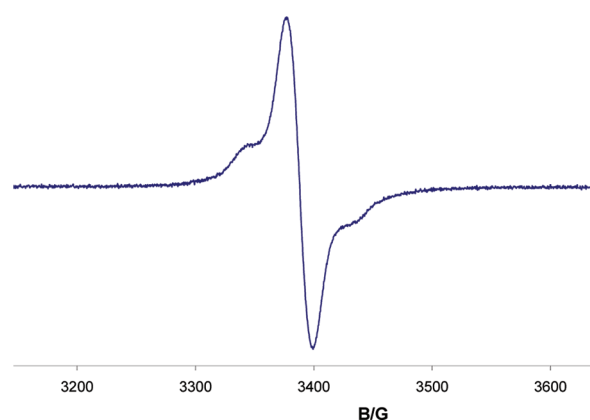


Figure 7. X-band, CH₂Cl₂ solution spectrum of [3]PF₆ (recorded as a first derivative at 243 K). *g*_{iso} = 1.991.

features assigned to coupling to ^{95/97}Mo, no hyperfine data could be extracted from the spectrum; attempts to improve resolution by variable-temperature investigations (193–303 K) and frequency variation (X-, S-, Q-band) were unsuccessful.

The poor resolution of the EPR spectrum of [3]PF₆ is in contrast to all other radicals derived from vinyl complexes of this metal–ligand system. However, the broad character of the spectrum can be rationalized in terms of an electron transfer rate between the two metal centers of [3]PF₆ that is comparable with the X-band EPR time scale. In support of this interpretation, the hyperfine coupling to ^{95/97}Mo was estimated from both X- and S-band spectra as approximately 16 G, around one-half of the typical value of *A*_{iso} (^{95/97}Mo) in monometallic radicals of the type [Mo{(C≡C)_nR}(dppe)(η-C₇H₇)]⁺. On the basis of the EPR investigations, the intramolecular electron transfer rate in [3]PF₆ is estimated to lie in the range 10⁸–10¹⁰ s⁻¹. This is slower than solvent reorientation frequencies (10¹¹–10¹² s⁻¹) and typical bond vibration frequencies (10¹³–10¹⁴ s⁻¹) consistent with the observed, valence-localized NIR and IR properties of [3]PF₆ (pronounced solvatochromic shifts and two IR-active bridging ligand vibrational modes).

The dication [3][PF₆]₂ was also investigated by EPR spectroscopy to probe the position of the thermal equilibrium between singlet and triplet configurations. In selected cases of all-carbon-bridged bimetallic dications, where the singlet/triplet energy gap is relatively small,^{7,53} EPR spectra with accompany-

ing half-field signals have been observed, although the spectra are broadened as a consequence of multiple unpaired electrons in the molecule, which greatly shorten relaxation times. The X-band EPR spectra of isolated samples of $[3][PF_6]_2$, which exhibit a strong, well-resolved signal [g_{iso} 1.996; $A_{iso}(^{95/97}Mo)$ 32 G; $A_{iso}(^{31}P)$ 23 G; $A_{iso}(H)$ 4.3 G] when recorded in solution in CH_2Cl_2 over the temperature range 213–243 K, are therefore not consistent with a thermally populated triplet diradical state. Instead the observed spectra are indicative of the presence of a monometallic $S = 1/2$ impurity within the sample of $[3][PF_6]_2$. Variable-temperature EPR studies on frozen solution or solid-state samples of $[3][PF_6]_2$ in the temperature range 80–5 K demonstrated the retention of the EPR signature characteristic of the paramagnetic $S = 1/2$ species, and in consequence, it was not possible to explore the behavior of weak, broad signals expected to arise from the triplet configuration of $[3][PF_6]_2$.

To probe further the energy gap between singlet and thermally populated triplet states of $[3][PF_6]_2$, magnetic susceptibility measurements were carried out on polycrystalline samples of $[3][PF_6]_2$ in the temperature range 2–300 K, under applied magnetic fields of 1 and 5 kG. The results, which are plotted as χ_M vs T and $\chi_M T$ vs T in Figure 8 (χ_M = molar

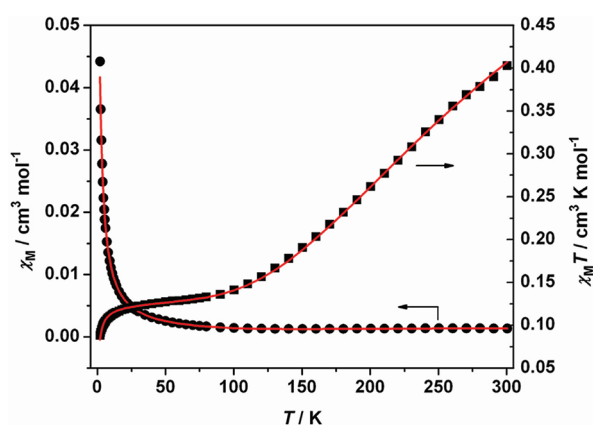


Figure 8. Plots of χ_M (●●●) and $\chi_M T$ (■ ■ ■) vs T for compound $[3][PF_6]_2$. The solid line represents the best fit of experimental data to eq 1 (see text).

magnetic susceptibility), demonstrate strong antiferromagnetic coupling between the unpaired electrons of the two Mo centers in $[3][PF_6]_2$, which leads to a diamagnetic ground state below 80 K and a thermally accessible paramagnetic triplet state.

As seen in Figure 8, the room-temperature $\chi_M T$ value is $0.4 \text{ cm}^3 \text{ K mol}^{-1}$, which is much smaller than the expected value of $0.75 \text{ cm}^3 \text{ K mol}^{-1}$ for two $S = 1/2$ uncorrelated spins (assuming $g = 2$). Upon cooling, $\chi_M T$ decreases rapidly to reach a plateau of ca. $0.12 \text{ cm}^3 \text{ K mol}^{-1}$ in the temperature range 80–20 K, after which it decreases again to a value of $0.09 \text{ cm}^3 \text{ K mol}^{-1}$ at 2 K. This behavior is characteristic of a large singlet–triplet energy gap. The plateau of $\chi_M T$ (or the increase of the magnetic susceptibility, χ_M) below 100 K is due to the proportion, ρ , of an uncoupled, monometallic paramagnetic impurity, in accord with the experimental EPR spectra; related uncoupled impurities have also been noted for the di-iron complexes $[\{Fe(dppe)Cp^*\}_2(\mu-C_4)][PF_6]_2$ and $[\{Fe(dppe)Cp^*\}_2(\mu-1,4\text{-diethynylbenzene})][PF_6]_2$.^{54,55} The experimental data were therefore fitted using the Bleaney–Bowers equation (1),⁵⁶ modified to take into account paramagnetic impurities

assumed to be monometallic Mo species with $S = 1/2$.

$$\chi_M = \frac{2Ng^2\beta^2}{k_B(T - \theta)} \frac{1}{3 + \exp(-J/k_B T)} (1 - \rho) + \frac{Ng^2\beta^2}{2k_B(T - \theta)} \rho + \text{TIP} \quad (1)$$

In eq 1, J represents the exchange coupling constant that accounts for magnetic coupling between Mo(1) and Mo(2) (i.e., the singlet–triplet energy gap) and N , g , k_B , and β represent the Avogadro number, the Zeeman factor, the Boltzmann constant, and the Bohr magneton, respectively. A Weiss constant θ was incorporated into the analysis to take account of weak intermolecular interactions that occur at low temperatures, and a correction was also made for temperature-independent paramagnetism (TIP). The best fit of both χ_M and $\chi_M T$, using eq 1 gave $J = -406 \pm 3 \text{ cm}^{-1}$, $\theta = -0.95 \pm 0.02 \text{ K}$, and $\rho = 0.16$, with $g = 1.996$ (fixed, based on EPR studies), $R(\chi_M T) = \sum(\chi_M T^{\text{obs}} - \chi_M T^{\text{calc}})^2 / \sum(\chi_M T^{\text{obs}})^2 = 3.1 \times 10^{-6}$, and $\text{TIP} = 120 \times 10^{-6} \text{ cm}^3 \text{ mol}^{-1}$. The results show that the magnetic interaction between Mo(1) and Mo(2) is antiferromagnetic, with a large exchange coupling constant ($J = -406 \text{ cm}^{-1}$) and a corresponding singlet–triplet energy gap ($\Delta G_{ST} = 406 \text{ cm}^{-1}$). The singlet–triplet energy gap determined for $[3][PF_6]_2$ is much larger than values reported for $[\{Fe(dppe)Cp^*\}_2(\mu-C_4)][PF_6]_2$ ($\Delta G_{ST} = 18 \text{ cm}^{-1}$)^{53,54} and $[\{Wl(dppe)\}_2(\mu-C_4)][PF_6]_2$ ($\Delta G_{ST} = 167 \text{ cm}^{-1}$)¹⁴ but rather smaller than that of the ruthenium complex $[\{Ru(dppe)Cp^*\}_2(\mu-C_4)][PF_6]_2$ ($\Delta G_{ST} = 850 \text{ cm}^{-1}$).¹⁷ Singlet–triplet energy gaps with magnitudes greater than 700 cm^{-1} are generally observed for 4d/5d metal centers linked by a C_4 bridge;⁵³ the smaller J value observed for $[3][PF_6]_2$ is consistent with differences in electronic structure (see below).

Electronic Structure Calculations. The compound $[\{Mo(dHpe)(\eta-C_7H_7)\}_2(\mu-C\equiv C\equiv C)]$ (3-H) was used to model complex 3, with geometry optimization and electronic structure calculations being carried out with the B3LYP/LANL2DZ functional and basis set combination in line with literature precedence and management of computational effort. The geometry was optimized with no symmetry restrictions and confirmed to be a minimum energy conformation by the lack of imaginary frequencies. The optimized geometry of 3-H (Table 6) correlates well with the expected butadiyndiyl

Table 6. Selected Calculated Bond Lengths for 3-H

bond	3-H (Å)
Mo(1)–C(α)	2.089
C(α)–C(β)	1.260
C(β)–C(β')	1.373
C(β')–C(α')	1.260
C(α')–Mo(2)	2.087
Mo(1)–P	2.544, 2.544
Mo(2)–P	2.546, 2.533

valence description with an alternating pattern of single and triple bonds across the length of the four-carbon chain and bond parameters at each molybdenum center similar to those calculated elsewhere²⁹ for alkynyl complexes of the Mo(dppe)-($\eta-C_7H_7$) auxiliary. The Mo(dHpe)($\eta-C_7H_7$) fragments are disposed in a *gauche* arrangement with the angle $Ct(1)\text{---}Mo\cdots Mo\text{---}Ct(2) = -82.7^\circ$. The energies and composition of

Table 7. Energy and % Composition of the Frontier Orbitals in the Calculated Complex 3-H

MO	energy/eV	Mo(1)	C(α)	C(β)	C ₇ H ₇ (1)	dHpe(1)	Mo(2)	C(α')	C(β')	C ₇ H ₇ (2)	dHpe(2)	M ₂	C ₄
LUMO	-0.76	18	1	0	33	12	11	0	1	18	6	29	2
HOMO	-3.67	24	11	10	7	2	17	12	8	8	2	41	41
HOMO-1	-3.74	17	12	8	9	2	24	11	9	7	2	41	40
HOMO-2	-4.27	39	4	0	5	4	15	2	8	20	3	54	14

the key frontier orbitals (LUMO, HOMO, HOMO-1, and HOMO-2) are set out in Table 7, and plots of HOMO and HOMO-1 of 3-H are presented in Figure 9.

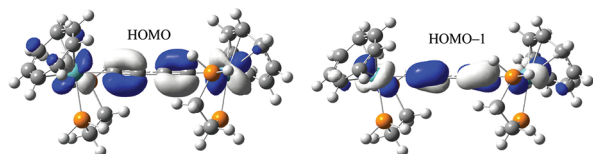


Figure 9. HOMO and HOMO-1 of 3-H at B3LYP/LANL2DZ plotted as an isosurface of 0.04 au.

The HOMO and HOMO-1 of 3-H have very similar compositions of metal (41%) and C₄ carbon bridge (40–41%) character. They are almost degenerate in energy and well removed from the other frontier orbitals (Table 7). Taking the Mo–Ct and Mo–C(α) vectors as approximating the z- and x-axes, respectively, to define a local coordinate system at each metal center, these orbitals feature an essentially d_{z²}/C₄(π)/d_{z²} structure (for both HOMO and HOMO-1, the identity of one of the metal orbitals is less clearly defined, but assignment as d_{z²} is indicated by the alignment of the principal orbital lobe along the z-axis toward the center of the C₇H₇ ring). The HOMO and HOMO-1 of 3-H (Figure 9) may be compared with the equivalent molecular orbitals of [$\{\text{Ru}(\text{dHpe})\text{Cp}\}_2(\mu\text{-C}\equiv\text{C}-\text{C}\equiv\text{C})$] (see Figure 1). The C₄ bridge orbitals for the two systems are essentially identical, but a key distinction is the identity of the frontier metal orbitals contributing to the interaction with the bridge orbitals. Thus the efficient in-plane interactions of [$\{\text{Ru}(\text{dHpe})\text{Cp}\}_2(\mu\text{-C}\equiv\text{C}-\text{C}\equiv\text{C})$] are replaced in 3-H by a symmetry-constrained overlap between the π orbitals of the C₄ bridge and the d_{z²}-based frontier orbitals of the Mo(dppe)($\eta\text{-C}_7\text{H}_7$) fragment. As a result, the HOMO and HOMO-1 of 3-H are strongly metal based in character (Table 7); for comparison DFT calculations on [$\{\text{M}(\text{dHpe})\text{Cp}\}_2(\mu\text{-C}\equiv\text{C}-\text{C}\equiv\text{C})$] (M = Fe, Ru) using the ADF⁵⁷ program report the % metal to % C₄ chain character in the HOMO of these systems as follows: M = Fe: M₂, 41%, C₄, 46%; M = Ru: M₂ = 26%, C₄ = 62% (see Figure 1).¹⁷

Attempts to model the oxidized complexes [3]PF₆ and [3][PF₆]₂ to reflect accurately the observed experimental properties of these systems were not successful at the levels of theory employed; higher levels of theory were not explored for these open-shell systems on the grounds of computational expense, and accurate computational modeling of localized mixed valence systems remains a significant challenge.¹⁹ However, it is suggested that the weak electronic coupling between metal centers in the mixed valence monocation [3]PF₆ can be attributed to the modest interaction between d_{z²}-based metal frontier orbitals and the all-carbon bridge; a related, symmetry-restricted interaction between the metal center and C₄ bridge has been proposed for [$\{\text{Wl}(\text{dppe})_2\}_2(\mu\text{-C}_4)$]ⁿ⁺.¹⁴ By contrast, on the basis of the large value of the exchange coupling constant *J* (−406 ± 3 cm^{−1}), the magnetic interaction

through the C₄ bridge in the dication [3][PF₆]₂ is more significant. This feature may originate from a HOMO in [3][PF₆]₂ related to HOMO-1 of [Mo(C≡CPh)(dppe)($\eta\text{-C}_7\text{H}_7$)] (Figure 2), which exhibits efficient in-plane overlap between the metal and carbon chain orbitals.²⁹ Nevertheless the *J* value for [3][PF₆]₂ is less than one-half of that determined for [$\{\text{Ru}(\text{dppe})\text{Cp}^*\}_2(\mu\text{-C}_4)$][PF₆]₂, and this may correlate with greater spin density at the metal centers in the Mo system.^{17,53}

DISCUSSION

Symmetrical all-carbon-bridged complexes of the type [$\{\text{L}_x\text{M}\}(\mu\text{-C}_4)\{\text{ML}_x\}$]ⁿ⁺ are known for a wide range of metal end-caps ML_x. Important distinctions between the redox chemistry of these systems, manifest in the spectroscopic and structural properties of the dications, may be observed dependent upon the identity of the metal end-cap. However, nearly all examples of the mixed valence monocations (*n* = 1) feature either fast electron transfer within the framework of two-state mixed valence complexes, delocalization, or significant ligand-based redox chemistry. In this context, the properties of [3]PF₆, as evidenced by IR, NIR, and EPR investigations, are clearly distinct such that the series of complexes [$\{\text{Mo}(\text{dppe})(\eta\text{-C}_7\text{H}_7)\}_2(\mu\text{-C}_4)$]ⁿ⁺ represent a separate subclass within the chemistry of [$\{\text{L}_x\text{M}\}(\mu\text{-C}_4)\{\text{ML}_x\}$]ⁿ⁺ systems.

Taken as a group, the spectroscopic properties of [3]PF₆ are indicative of a localized electronic structure, and in terms of the classical two-state model for charge transfer transitions,^{28,49} [3]PF₆ appears to rest firmly in the class II region. However, the observed characteristics of the NIR spectrum of [3]PF₆ cannot be fully rationalized by a conventional Hush-style two-state analysis. It has been suggested that the two-state model has serious limitations where bridge orbitals are significantly involved in the semioccupied molecular orbitals of the mixed valence system,¹¹ a circumstance that, on the basis of spectroscopic and DFT investigations,^{16,17} clearly applies to many complexes of the type [$\{\text{L}_x\text{M}\}(\mu\text{-C}_4)\{\text{ML}_x\}$]ⁿ⁺. An alternative three-state model,^{49,51,58–61} in which electron transfer can be mediated through the additional mixing of a third electronic state involving the bridging ligand, may have some validity for these systems. Depending on the relative energies of product/reactant versus bridge states, electron transfer may occur through a superexchange or hopping process; in the superexchange mechanism, the bridge acts only to mediate donor and acceptor wave functions, whereas in the hopping mechanism, the electron is actually located at the bridge for a short period in its passage from one redox center to the other.⁵⁸ The key spectral features of the theoretical three-state model, which distinguish it from the classical two-state treatment of mixed valence systems, are (i) a reduction in bandwidth $\Delta\nu_{1/2}$ of IVCT bands for a given value of electronic coupling and (ii) an additional absorption to high energy of the IVCT band originating from a MLCT/LMCT transition; in the class II region, the intensity of this band initially increases with increased electronic coupling but then decreases to zero as the class II/class III borderline is approached.⁴⁹ For this reason, the

NIR spectrum of a weakly coupled, symmetrical class II system such as $[3]PF_6$ presents an opportunity to investigate experimentally the validity of a three-state model for electron transfer in all-carbon-bridged organometallics because the simultaneous observation of IVCT and MLCT/LMCT transitions, diagnostic of the model, may be possible.

The experimental NIR spectrum of $[3]PF_6$ can be interpreted in terms of the predicted spectral characteristics of a bridge-mediated, three-state model for electron transfer in a weakly coupled, symmetrical mixed valence complex as outlined below. The observation of three IVCT bands (at 3200, 4400, and 9300 cm^{-1} in CH_2Cl_2) in the experimental spectrum of $[3]PF_6$ is readily explained by the nondegeneracy of the metal d orbitals arising from strong π and δ interactions with the C_7H_7 ring in the $Mo(dppe)(\eta-C_7H_7)$ end-cap units.²⁹ Each of the three observed IVCT bands exhibits a $\Delta\nu_{1/2}$ parameter narrower than predicted by the classical two-state analysis in accord with a three-state interpretation. However the key issue is the assignment of the fourth band in the NIR region at 8500 cm^{-1} (distinguished by its narrow bandwidth, relatively high intensity, and very small solvatochromic shift). One possible interpretation is that this much sharper and intense absorption originates from an LMCT process from the bridging ligand. The observation of this band is an integral part of the predictions of a three-state model for electron transfer in a weakly coupled class II system, and it may be noted that an analogous absorption is not seen in the NIR spectrum of the more weakly coupled 1,12-bis(ethynyl)-1,12-carborane-bridged analogue $[\{Mo(dppe)(\eta-C_7H_7)\}_2(\mu-1,12-(C\equiv C)_2-1,12-C_2B_{10}H_{10})]^+$, where the energies of the carborane bridge π and π^* levels are well removed from the metal orbitals in the frontier region.⁶² Experimental evidence for the simultaneous observation of IVCT and MLCT/LMCT transitions in the NIR spectra of all-carbon-bridged organometallic systems is very limited,⁶³ possibly because the strong electronic coupling, characteristic of these complexes, leads to zero intensity of the MLCT/LMCT transition or because the individual components of the spectra are superimposed and cannot be reliably identified. The design of further examples of weakly coupled, symmetrical all-carbon-bridged complexes may therefore be a useful strategy in the study of the mechanism of intervalence electron transfer in these systems.

CONCLUSIONS

Oxidative coupling of $[Mo(C\equiv CH)(dppe)(\eta-C_7H_7)]$ to give $[\{Mo(dppe)(\eta-C_7H_7)\}_2(\mu-C\equiv CH-CH\equiv C)]PF_6$ followed by deprotonation affords mixed valence all-carbon-bridged $[\{Mo(dppe)(\eta-C_7H_7)\}_2(\mu-C_4)]PF_6$, $[3]PF_6$, as a mixture with neutral $[\{Mo(dppe)(\eta-C_7H_7)\}_2(\mu-C\equiv C-C\equiv C)]$, **3**. Electrochemical investigations reveal a series of redox processes indicative of the formation of $[\{Mo(dppe)(\eta-C_7H_7)\}_2(\mu-C_4)]^{n+}$ ($n = 0, 1, 2, 3, 4$), and the redox states $n = 0, 1$, and 2 have been isolated and characterized. Spectroscopic investigations on $[3]PF_6$ by IR, Raman, NIR, and EPR spectroscopy uncover properties characteristic of a localized mixed valence system with an intramolecular electron transfer rate comparable with the X-band EPR time scale (10^8 – 10^{10} s^{-1}). This behavior contrasts with the properties of most previously reported mixed valence $[\{L_xM\}(\mu-C_4)\{ML_x\}]^+$ systems, for which either a fully delocalized electronic structure or bridge-centered redox chemistry is observed. The weak electronic coupling observed for $[3]PF_6$ presents the opportunity to examine the validity of a three-state model for electron transfer that involves a third state

formed by charge transfer to or from the bridging C_4 ligand. Analysis of the experimental NIR spectrum of $[3]PF_6$ reveals a good correlation with the predicted spectral properties for a three-state model description of electron transfer in a weakly coupled, symmetrical mixed valence system. The dicationic complex $[\{Mo(dppe)(\eta-C_7H_7)\}_2(\mu-C_4)]PF_6$, $[3]PF_6$, exhibits strong antiferromagnetic coupling with a singlet/triplet energy gap of 406 cm^{-1} . However the magnitude of the magnetic coupling in $[3]PF_6$ is less than one-half of that reported for $[\{Ru(dppe)Cp^*\}_2(\mu-C_4)]PF_6$, and X-ray structural data for $[3]PF_6$ are not consistent with significant cumulenyl character in the C_4 bridge. Overall the properties of $[\{Mo(dppe)(\eta-C_7H_7)\}_2(\mu-C_4)]^{n+}$ are atypical of all-carbon-bridged bimetallics of 4d/5d metals with both electronic and magnetic coupling through the C_4 bridge weaker than expected. The electronic structure of the $Mo(dppe)(\eta-C_7H_7)$ end-cap, which serves to enhance the metal-based character of frontier orbitals, appears to play an important role in regulating the magnitude of through-bridge interactions in these complexes.

EXPERIMENTAL SECTION

General Procedures. The preparation, purification, and reactions of the complexes described were carried out under dry nitrogen. All solvents were dried by standard methods, distilled, and deoxygenated before use. The complex $[MoBr(dppe)(\eta-C_7H_7)]\cdot 0.5CH_2Cl_2$ was prepared by a published procedure.³⁷ NMR spectra were recorded in CD_2Cl_2 unless stated otherwise on a Varian Inova 400 (400 MHz 1H , 100 MHz $^{13}C\{^1H\}$, 162 MHz $^{31}P\{^1H\}$) spectrometer. Solution infrared spectra were obtained on a Perkin-Elmer FT RX1 spectrometer, and solid-state spectra were recorded on a Thermo-scientific Nicolet iS5 spectrometer with ATR fitment; MALDI mass spectra were recorded using a Micromass/Waters ToF Spec 2E instrument. Microanalyses were conducted by the staff of the Microanalytical Service of the School of Chemistry, University of Manchester. Cyclic voltammograms were recorded ($\nu = 100$ mV s^{-1}) from 0.2 M $[Bu_4N]PF_6/CH_2Cl_2$ solutions ca. 1×10^{-4} M in analyte using a three-electrode cell equipped with a glassy carbon disk working electrode, Pt wire counter electrode, and Ag/AgCl reference electrode, and data were collected on an Autolab PG-STAT 30 potentiostat. All redox potentials are reported with reference to an internal standard of the ferrocene/ferrocenium couple ($FeCp_2/[FeCp_2]^+ = 0.00$ V). UV–vis–NIR and IR spectroelectrochemical experiments were performed at room temperature with an airtight OTTL cell of Hartl design⁶⁴ equipped with Pt minigrd working and counter electrodes, a Ag wire reference electrode, and CaF_2 windows using either a Nicolet Avatar spectrometer or a Perkin-Elmer Lambda 900 spectrophotometer. Raman spectra were recorded using a Horiba Jobin-Yvon LabRamHR, equipped with a 633 nm laser, augmented by additional 532 nm (Coherent DPSS) and 785 nm (Sacher) excitation lasers. The instrument was calibrated using a neon lamp, and the Raman shifts are reported to an accuracy of ± 1 cm^{-1} . EPR experiments were conducted on a Bruker BioSpin EMX microspectrometer; spectra are the average of 16 scans. Spectral analysis and simulation was carried out using Bruker WinEPR software (Bruker Biospin Ltd.). Magnetic susceptibility measurements were carried out on polycrystalline samples in the temperature range 2–300 K, using a Quantum Design MPMS XL SQUID magnetometer equipped with a 7 T magnet. Experimental magnetic data were corrected for the diamagnetism of the ligands by using Pascal constants and for the magnetic contribution of the sample holder by measurement.

Preparation of $[Mo(C\equiv CH_2)(dppe)(\eta-C_7H_7)]PF_6$. A mixture of $[MoBr(dppe)(\eta-C_7H_7)]\cdot 0.5CH_2Cl_2$ (1.50 g, 2.12 mmol), KPF_6 (0.82 g, 4.46 mmol), and $HC\equiv CSiMe_3$ (1.04 g, 10.61 mmol) in methanol (50 cm^3) was heated at reflux for 3 h. The reaction mixture was reduced in volume to ca. 20 cm^3 , resulting in the formation of an orange precipitate, and then cooled to -20 $^\circ C$ for 1 h. The precipitate was collected and recrystallized from CH_2Cl_2 /diethyl ether to give the

product as an orange solid, which was dried *in vacuo* (yield: 1.11 g (69%)) and identified by comparison with an authentic sample.³⁶

Preparation of [Mo(C≡CH)(dppe)(C₇H₇)]₂, 1. [Mo(C≡CH)₂(dppe)(η-C₇H₇)]PF₆ (1.08 g, 1.43 mmol) was suspended in thf (30 cm³) and cooled to -30 °C. KOBu^t (1.28 g, 11.42 mmol) was added, and the mixture was stirred at -30 °C for 10 min and then at room temperature for 1 h. The resulting brown solution was evaporated to dryness, and the residue dissolved in CH₂Cl₂ (ca. 20 cm³) and stirred for 5 min. The resulting suspension was filtered through a Celite pad (2 cm diameter × 2.5 cm deep), and the filtrate treated with hexane. The volume of the solution was then reduced to give a brown precipitate, which was collected, washed with hexane, and dried *in vacuo*; yield 685 mg (78%). ¹H NMR: δ 1.74, t, J(P-H) 4 Hz, 1H, C≡CH; 1.88, m, 2H, CH₂; 2.50, m, 2H, CH₂; 4.68, s, 7H, C₇H₇; 7.22–7.73, m, 20H, Ph. ¹³C{¹H} NMR: 140.2, m, 135.8, m, Ph; 133.3, m, 131.3, m, Ph_o; 130.1, t, J(P-C) 25 Hz, C_o; 128.8, s, 128.4, s, Ph_i; 127.6, m, 127.1, m, Ph_m; 104.3, s, C_β; 86.5, s, C_γH₇; 25.8, m, CH₂ (dppe). ³¹P{¹H} NMR: δ 63.8 (s, dppe). IR (CH₂Cl₂): ν(C≡C) 1908 cm⁻¹, ν(C₂-H) 3265 cm⁻¹. MALDI-MS (*m/z*): 612 [M]⁺. Anal. Calcd (%) for C₃₅H₃₂MoP₂: C, 68.9; H, 5.3. Found: C, 68.2; H, 5.3.

Preparation of [Mo(dppe)(η-C₇H₇)]₂(μ-C≡CH-CH=C)[PF₆]₂, [2]-[PF₆]₂. To a cooled solution (-78 °C) of [Mo(C≡CH)(dppe)(η-C₇H₇)] (600 mg, 0.980 mmol) in thf (5 cm³) was added [FeCp₂]₂PF₆ (308 mg, 0.931 mmol). The reaction mixture was stirred at -78 °C for 5 h to give a deep purple solution. Addition of diethyl ether (30 cm³) resulted in precipitation of the crude product as a deep purple solid. Recrystallization from CH₂Cl₂/diethyl ether allowed separation of the more soluble side-product [Mo(C≡CH)(dppe)(η-C₇H₇)]PF₆ from the required complex [2][PF₆]₂, which precipitated from the solution first; yield 594 mg (80%). ¹H NMR: δ 2.33, m, 4H, CH₂; 2.51, m, 4H, CH₂; 4.41, t, br, 2H, J(H-P) ≈ 11 Hz, C≡CH; 5.07, s, 14H, C₇H₇; 7.16–7.71, m, 40H, Ph. ¹³C{¹H} NMR: 134.4, 132.1, 131.1, 129.6, 129.5, Ph (dppe); 108.3 C_β; 93.2, C_γH₇; 27.8, m, CH₂ (dppe). ³¹P NMR: δ 51.3 (s, dppe). IR (CH₂Cl₂): ν(C=C) 1556 cm⁻¹. Anal. Calcd (%) for C₇₀H₆₄Mo₂P₆F₁₂: C, 55.6; H, 4.3. Found: C, 55.1; H, 4.2.

Preparation of [Mo(dppe)(η-C₇H₇)]₂(μ-C≡C-C≡C), 3, and [Mo(dppe)(η-C₇H₇)]₂(μ-C₄)PF₆, [3]PF₆. [Mo(dppe)(η-C₇H₇)]₂(μ-C≡CH-CH=C)[PF₆]₂ (580 mg, 0.384 mmol) was dissolved in thf (30 cm³), and KOBu^t (172 mg, 1.536 mmol) was added to the solution; the resulting green-brown suspension was then stirred at room temperature for 5 h before evaporating to dryness. The residue was dissolved in CH₂Cl₂ (20 cm³) and filtered through a pad of Celite, and the filtrate evaporated to dryness. The resulting residue was washed with toluene (20 cm³), and the washings were removed and retained. The remaining toluene-insoluble material was dried, then recrystallized from CH₂Cl₂/hexane to give [3]PF₆ as a brown solid, which was collected, washed with further hexane, and dried *in vacuo*; yield 230 mg (44%). IR (CH₂Cl₂): ν(C≡C) 1930, 1868 cm⁻¹. MALDI-MS (*m/z*): 1220 [M]⁺. Anal. Calcd (%) for C₇₀H₆₂Mo₂P₆F₆: C, 61.6; H, 4.6. Found: C, 61.9; H, 4.8. The mother liquors remaining from the isolation of [3]PF₆ and the toluene washings were combined and evaporated to dryness. The resulting residue was extracted with toluene and filtered through a pad of Celite, and the solvent removed. Fractional recrystallization of the residue from CH₂Cl₂/hexane led first to precipitation of residual [3]PF₆ to leave an orange-brown solution, which on reduction in volume and addition of further hexane yielded 3 as an orange-brown solid; yield 0.025 g (5%). MALDI-MS (*m/z*): 1220 [M]⁺. Anal. Calcd (%) for C₇₀H₆₂Mo₂P₄: C, 69.0; H, 5.1. Found: C, 69.4; H, 5.3.

Preparation of [Mo(dppe)(η-C₇H₇)]₂(μ-C₄)[PF₆]₂, [3][PF₆]₂. A brown-green solution of [Mo(dppe)(η-C₇H₇)]₂(μ-C₄)PF₆ (83 mg, 0.061 mmol) in CH₂Cl₂ (20 cm³) was treated with [FeCp₂]₂PF₆ (44 mg, 0.133 mmol). The reaction mixture was stirred for 20 min, resulting in the formation of an intense green solution, which was filtered through Celite, reduced in volume, and treated with diethyl ether to precipitate the product as an emerald green solid; yield 57 mg (62%). MALDI-MS (*m/z*): 1220 [M]⁺. Anal. Calcd (%) for C₇₀H₆₂Mo₂P₆F₁₂: C, 55.7; H, 4.1. Found: C, 54.8; H, 4.0.

Computational Details. All calculations were carried out using the Gaussian 03 package.⁶⁵ The model geometry of 3-H was optimized using B3LYP⁶⁶ and MPW1K,^{67,68} with no symmetry constraints. The pseudopotential LANL2DZ^{69–71} was used for all atoms. Frequency calculations were carried out on these optimized geometries at the corresponding levels and shown to have no imaginary frequencies. Molecular orbital computations were carried out on these optimized geometries at the same level of theory and displayed using Gauss View 4.1.⁷² The orbital compositions were generated with the aid of GaussSum.⁷³

X-ray Crystal Structure of [Mo(dppe)(η-C₇H₇)]₂(μ-C₄)[PF₆]₂, [3][PF₆]₂. Single crystals of [3][PF₆]₂ were obtained as brown-green blocks by vapor diffusion of diethyl ether into a MeCN solution of the complex, and a crystal of dimensions 0.40 × 0.30 × 0.20 mm was selected for analysis. Single-crystal X-ray data were collected at 100 K on an Oxford Diffraction X-Calibur 2 diffractometer equipped with an Oxford-Cryosystems low-temperature device, by a means of Mo Kα (λ = 0.71069 Å) radiation and ω scans. Data were corrected for Lorentz, polarization, and absorption factors. Data collection, cell refinement, and data reduction were carried out with CrysAlis CCD and CrysAlis RED, Oxford Diffraction Ltd. software; SHELXS-97⁷⁴ was employed for computing the structure solution, and SHELXL-97⁷⁵ for computing structure refinement. The structure was solved by direct methods with refinement based on F². The asymmetric unit of [3][PF₆]₂ contains the Mo complex, two PF₆ counteranions, one ordered MeCN solvent of crystallization, and a disordered solvent fragment defined as 2 MeCN molecules at 0.25 occupancy and one H₂O at 0.25 occupancy. Except as detailed below, all non-hydrogen atoms were refined anisotropically; hydrogen atoms were included in calculated positions, except those of the disordered solvent. A phenyl group of a dppe ligand C(51)–C(56) and a PF₆ counterion, P(2s), F(7s)–F(12s), were disordered. The disordered component of the Ph group has been constrained to be a regular hexagon, and there are restraints on the geometry of the disordered PF₆ and some of the anisotropic displacement parameters. The anisotropic displacement parameters of the C(1)–C(7) atoms in the cycloheptatrienyl ring were disordered and restrained since they tended to become unrealistic.

Crystal Data for [3][PF₆]₂: C₇₀H₆₇Mo₂N_{1.5}O_{0.25}P₆F₁₂, M_r = 1574.98, monoclinic, space group C2/c, a = 58.826(3) Å, b = 11.7374(9) Å, c = 19.7396(11) Å, β = 97.174(5)°, U = 13522.9(15) Å³, Z = 8, μ = 0.591 mm⁻¹, 11 910 reflections collected, final wR₂(F²) = 0.1260 for all data, conventional R₁ = 0.0605 for 6051 reflections with I > 2σ(I), completeness to theta = 99.8%.

■ ASSOCIATED CONTENT

● Supporting Information

Cyclic voltammogram of [3]PF₆, Raman spectra of [3]ⁿ⁺ (n = 0, 1, 2), ATR infrared spectra of solid-state samples of [3]ⁿ⁺ (n = 1, 2), expansion of plots of χ_M and χ_MT vs T for [3][PF₆]₂. CIF files giving crystallographic data for complex [3][PF₆]₂. This material is available free of charge via the Internet at <http://pubs.acs.org>.

■ AUTHOR INFORMATION

Corresponding Author

*E-mail: p.j.low@durham.ac.uk; Mark.Whiteley@manchester.ac.uk.

■ ACKNOWLEDGMENTS

We thank the EPSRC for support of this work through grants EP/E025544/1 and EP/E02582X/1. P.J.L. holds an EPSRC Leadership Fellowship.

■ REFERENCES

- (1) Paul, F.; Lapinte, C. *Coord. Chem. Rev.* **1998**, 178–180, 431.
- (2) Bruce, M. I.; Low, P. J. *Adv. Organomet. Chem.* **2004**, 50, 179.

- (3) Carroll, R. L.; Gorman, C. B. *Angew. Chem., Int. Ed.* **2002**, *41*, 4378.
- (4) Low, P. J. *Dalton Trans.* **2005**, 2821.
- (5) Le Narvor, N.; Toupet, L.; Lapinte, C. *J. Am. Chem. Soc.* **1995**, *117*, 7129.
- (6) Guillemot, M.; Toupet, L.; Lapinte, C. *Organometallics* **1998**, *17*, 1928.
- (7) (a) Brady, M.; Weng, W.; Zhou, Y.; Seyler, J. W.; Amoroso, A. J.; Arif, A. M.; Böhme, M.; Frenking, G.; Gladysz, J. A. *J. Am. Chem. Soc.* **1997**, *119*, 775. (b) Herrmann, C.; Neugebauer, J.; Gladysz, J. A. *Inorg. Chem.* **2005**, *44*, 6174.
- (8) (a) Bruce, M. I.; Low, P. J.; Costuas, K.; Halet, J.-F.; Best, S. P.; Heath, G. A. *J. Am. Chem. Soc.* **2000**, *122*, 1949. (b) Bruce, M. I.; Denisovich, L. I.; Low, P. J.; Peregodova, S. M.; Ustynuk, N. A. *Mendeleev Commun.* **1996**, 200.
- (9) Bruce, M. I.; Ellis, B. G.; Low, P. J.; Skelton, B. W.; White, A. H. *Organometallics* **2003**, *22*, 3184.
- (10) Gao, L.-B.; Zhang, L.-Y.; Shi, L.-X.; Chen, Z.-N. *Organometallics* **2005**, *24*, 1678.
- (11) Bruce, M. I.; Costuas, K.; Davin, T.; Halet, J.-F.; Kramarczuk, K. A.; Low, P. J.; Nicholson, B. K.; Perkins, G. J.; Roberts, R. L.; Skelton, B. W.; Smith, M. E.; White, A. H. *Dalton Trans.* **2007**, 5387.
- (12) Bruce, M. I.; Kramarczuk, K. A.; Skelton, B. W.; White, A. H. *J. Organomet. Chem.* **2010**, *695*, 469.
- (13) Kheradmandan, S.; Heinze, K.; Schmalte, H. W.; Berke, H. *Angew. Chem., Int. Ed.* **1999**, *38*, 2270.
- (14) Semenov, S. N.; Blacque, O.; Fox, T.; Venkatesan, K.; Berke, H. *J. Am. Chem. Soc.* **2010**, *132*, 3115.
- (15) Paul, F.; Meyer, W. E.; Toupet, L.; Jiao, H.; Gladysz, J. A.; Lapinte, C. *J. Am. Chem. Soc.* **2000**, *122*, 9405.
- (16) Jiao, H.; Costuas, K.; Gladysz, J. A.; Halet, J.-F.; Guillemot, M.; Toupet, L.; Paul, F.; Lapinte, C. *J. Am. Chem. Soc.* **2003**, *125*, 9511.
- (17) Bruce, M. I.; Costuas, K.; Davin, T.; Ellis, B. G.; Halet, J.-F.; Lapinte, C.; Low, P. J.; Smith, M. E.; Skelton, B. W.; Toupet, L.; White, A. H. *Organometallics* **2005**, *24*, 3864.
- (18) Coat, F.; Guillevic, M.-A.; Toupet, L.; Paul, F.; Lapinte, C. *Organometallics* **1997**, *16*, 5988.
- (19) Costuas, K.; Rigaut, S. *Dalton Trans.* **2011**, *40*, 5643.
- (20) Xi, B.; Ren, T. C. R. *Chem.* **2009**, *12*, 321.
- (21) Ren, T. *Organometallics* **2005**, *24*, 4854.
- (22) Low, P. J.; Brown, N. J. *J. Cluster Sci.* **2010**, *21*, 235.
- (23) Semenov, S. N.; Taghipourian, S. F.; Blacque, O.; Fox, T.; Venkatesan, K.; Berke, H. *J. Am. Chem. Soc.* **2010**, *132*, 7584.
- (24) Ying, J.-W.; Liu, I.P.-C.; Xi, B.; Song, Y.; Campana, C.; Zuo, J.-L.; Ren, T. *Angew. Chem., Int. Ed.* **2010**, *49*, 954.
- (25) Woodworth, B. E.; White, P. S.; Templeton, J. L. *J. Am. Chem. Soc.* **1997**, *119*, 828.
- (26) Worth, G. H.; Robinson, B. H.; Simpson, J. *Organometallics* **1992**, *11*, 3863.
- (27) Ouddai, N.; Costuas, K.; Bencharif, M.; Saillard, J.-Y.; Halet, J.-F. *C. R. Chim.* **2005**, *8*, 1336.
- (28) (a) Robin, M. B.; Day, P. *Adv. Inorg. Chem. Radiochem.* **1967**, *10*, 247. (b) Hush, N. S. *Prog. Inorg. Chem.* **1967**, *8*, 391.
- (29) Brown, N. J.; Collison, D.; Edge, R.; Fitzgerald, E. C.; Helliwell, M.; Howard, J. A. K.; Lancashire, H. N.; Low, P. J.; McDouall, J. J. W.; Raftery, J.; Smith, C. A.; Yufit, D. S.; Whiteley, M. W. *Organometallics* **2010**, *29*, 1261.
- (30) Menconi, G.; Kaltsoyannis, N. *Organometallics* **2005**, *24*, 1189.
- (31) Tamm, M.; Kunst, A.; Bannenberg, T.; Herdtweck, E.; Schmid, R. *Organometallics* **2005**, *24*, 3163.
- (32) Elian, M.; Chen, M. M. L.; Mingos, D. M. P.; Hoffmann, R. *Inorg. Chem.* **1976**, *15*, 1148.
- (33) Iyer, R. S.; Selegue, J. P. *J. Am. Chem. Soc.* **1987**, *109*, 910.
- (34) (a) Beddoes, R. L.; Bitcon, C.; Ricalton, A.; Whiteley, M. W. *J. Organomet. Chem.* **1989**, *367*, C21. (b) Unseld, D.; Krivykh, V. V.; Heinze, K.; Wild, F.; Artus, G.; Schmalte, H.; Berke, H. *Organometallics* **1999**, *18*, 1525. (c) Fernández, F. J.; Venkatesan, K.; Blacque, O.; Alfonso, M.; Schmalte, H. W.; Berke, H. *Chem.—Eur. J.* **2003**, *9*, 6192. (d) Venkatesan, K.; Fox, T.; Schmalte, H. W.; Berke, H. *Organometallics* **2005**, *24*, 2834. (e) Valyaev, D. A.; Semeikin, O. V.; Ustynuk, N. A. *Coord. Chem. Rev.* **2004**, *248*, 1679. (f) Schauer, P. A.; Low, P. J. *Eur. J. Inorg. Chem.* **2011**, in press.
- (35) Bruce, M. I.; Costuas, K.; Ellis, B. G.; Halet, J.-F.; Low, P. J.; Moubarak, B.; Murray, K. S.; Ouddai, N.; Perkins, G. J.; Skelton, B. W.; White, A. H. *Organometallics* **2007**, *26*, 3735.
- (36) Beddoes, R. L.; Bitcon, C.; Grime, R. W.; Ricalton, A.; Whiteley, M. W. *J. Chem. Soc., Dalton Trans.* **1995**, 2873.
- (37) Grime, R. W.; Helliwell, M.; Hussain, Z. I.; Lancashire, H. N.; Mason, C. R.; McDouall, J. J. W.; Mydlowski, C. M.; Whiteley, M. W. *Organometallics* **2008**, *27*, 857.
- (38) Aston, G. M.; Badriya, S.; Farley, R. D.; Grime, R. W.; Ledger, S. J.; Mabbs, F. E.; McInnes, E. J. L.; Morris, H.; Ricalton, A.; Rowlands, C. C.; Wagner, K.; Whiteley, M. W. *J. Chem. Soc., Dalton Trans.* **1999**, 4379.
- (39) Lancashire, H. N.; Ahmed, R.; Hague, T. L.; Helliwell, M.; Hopgood, G. A.; Sharp, L.; Whiteley, M. W. *J. Organomet. Chem.* **2006**, *691*, 3617.
- (40) Denis, R.; Toupet, L.; Paul, F.; Lapinte, C. *Organometallics* **1999**, 4379.
- (41) Paul, F.; Ellis, B. G.; Bruce, M. I.; Toupet, L.; Roisnel, T.; Costuas, K.; Halet, J.-F.; Lapinte, C. *Organometallics* **2006**, *25*, 649.
- (42) Fox, M. A.; Roberts, R. L.; Khairul, W. M.; Hartl, F.; Low, P. J. *J. Organomet. Chem.* **2007**, *692*, 3277.
- (43) Bitcon, C.; Whiteley, M. W. *J. Organomet. Chem.* **1987**, *366*, 385.
- (44) Beddoes, R. L.; Bitcon, C.; Whiteley, M. W. *J. Organomet. Chem.* **1991**, *402*, 85.
- (45) (a) Bruce, M. I.; Hall, B. C.; Kelly, B. D.; Low, P. J.; Skelton, B. W.; White, A. H. *J. Chem. Soc., Dalton Trans.* **1999**, 3719. (b) Coat, F.; Lapinte, C.; Toupet, L.; Costuas, K.; Halet, J.-F. *J. Organomet. Chem.* **2003**, *683*, 368.
- (46) Brown, N. J.; Collison, D.; Edge, R.; Fitzgerald, E. C.; Low, P. J.; Helliwell, M.; Ta, Y. T.; Whiteley, M. W. *Chem. Commun.* **2010**, *46*, 225.
- (47) Demadis, K. D.; Hartshorn, C. M.; Meyer, T. J. *Chem. Rev.* **2001**, *101*, 2655.
- (48) D'Alessandro, D. M.; Keene, F. R. *Chem. Soc. Rev.* **2006**, *35*, 424.
- (49) Brunschwig, B. S.; Creutz, C.; Sutin, N. *Chem. Soc. Rev.* **2002**, *31*, 168.
- (50) Hush value for $\Delta n_{1/2}$ calculated from the equation $\Delta n_{1/2} = (2310n_{\max})^{1/2}$.
- (51) Lohan, M.; Justard, F.; Roisnel, T.; Ecorchard, P.; Lang, H.; Lapinte, C. *Organometallics* **2010**, *29*, 4804.
- (52) Carter, E.; Collison, D.; Edge, R.; Fitzgerald, E. C.; Lancashire, H. N.; Murphy, D. M.; McDouall, J. J. W.; Sharples, J.; Whiteley, M. W. *Dalton Trans.* **2010**, *39*, 11424.
- (53) Lapinte, C. *J. Organomet. Chem.* **2008**, *693*, 793.
- (54) Le Narvor, N.; Lapinte, C. *C. R. Acad. Sci. Ser. IIC: Chim.* **1998**, *745*.
- (55) Paul, F.; Bondon, A.; da Costa, G.; Malvolti, F.; Sinbandhit, S.; Cador, O.; Costuas, K.; Toupet, L.; Boillot, M.-L. *Inorg. Chem.* **2009**, *48*, 10608.
- (56) Bleaney, B.; Bowers, K. D. *Proc. R. Soc. London, Ser. A* **1952**, *214*, 451.
- (57) (a) *ADF2002.01, SCM, Theoretical Chemistry*; Vrije Universiteit: Amsterdam, The Netherlands, <http://www.scm.com>. (b) Guerra, C. F.; Snijders, J. G.; te Velde, G.; Baerends, E. J. *Theor. Chem. Acc.* **1998**, *99*, 391.
- (58) Lambert, C.; Nöll, G.; Schelter, J. *Nat. Mater.* **2002**, *1*, 69.
- (59) Lambert, C.; Amthor, S.; Schelter, J. *J. Phys. Chem. A* **2004**, *108*, 6474.
- (60) Amthor, S.; Lambert, C. *J. Phys. Chem. A* **2006**, *110*, 1177.
- (61) Londergan, C. H.; Kubiak, C. P. *J. Phys. Chem. A* **2003**, *107*, 9301.
- (62) Brown, N. J.; Lancashire, H. N.; Fox, M. A.; Collison, D.; Edge, R.; Yufit, D. S.; Howard, J. A. K.; Whiteley, M. W.; Low, P. J. *Organometallics* **2011**, *30*, 884.
- (63) Le Stang, S.; Paul, F.; Lapinte, C. *Organometallics* **2000**, *19*, 1035.

- (64) Krejcek, M.; Danek, M.; Hartl, F. J. *Electroanal. Chem.* **1991**, *317*, 179.
- (65) Frisch, M. J.; Trucks, G. W.; Schlegel, H. B.; Scuseria, G. E.; Robb, M. A.; Cheeseman, J. R.; Montgomery, J. A., Jr.; Vreven, T.; Kudin, K. N.; Burant, J. C.; Millam, J. M.; Iyengar, S. S.; Tomasi, J.; Barone, V.; Mennucci, B.; Cossi, M.; Scalmani, G.; Rega, N.; Petersson, G. A.; Nakatsuji, H.; Hada, M.; Ehara, M.; Toyota, K.; Fukuda, R.; Hasegawa, J.; Ishida, M.; Nakajima, T.; Honda, Y.; Kitao, O.; Nakai, H.; Klene, M.; Li, X.; Knox, J. E.; Hratchian, H. P.; Cross, J. B.; Bakken, V.; Adamo, C.; Jaramillo, J.; Gomperts, R.; Stratmann, R. E.; Yazyev, O.; Austin, A. J.; Cammi, R.; Pomelli, C.; Ochterski, J. W.; Ayala, P. Y.; Morokuma, K.; Voth, G. A.; Salvador, P.; Dannenberg, J. J.; Zakrzewski, V. G.; Dapprich, S.; Daniels, A. D.; Strain, M. C.; Farkas, O.; Malick, D. K.; Rabuck, A. D.; Raghavachari, K.; Foresman, J. B.; Ortiz, J. V.; Cui, Q.; Baboul, A. G.; Clifford, S.; Cioslowski, J.; Stefanov, B. B.; Liu, G.; Liashenko, A.; Piskorz, P.; Komaromi, I.; Martin, R. L.; Fox, D. J.; Keith, T.; Al-Laham, M. A.; Peng, C. Y.; Nanayakkara, A.; Challacombe, M.; Gill, P. M. W.; Johnson, B.; Chen, W.; Wong, M. W.; Gonzalez, C.; Pople, J. A. *Gaussian 03*, Revision C.02; Gaussian, Inc.: Wallingford, CT: 2004.
- (66) Becke, A. D. *J. Chem. Phys.* **1993**, *98*, 648.
- (67) Lynch, B. J.; Fast, P. L.; Harris, M.; Truhlar, D. G. *J. Phys. Chem. A* **2000**, *104*, 4811.
- (68) Lynch, B. J.; Zhao, Y.; Truhlar, D. G. *J. Phys. Chem. A* **2003**, *107*, 1384.
- (69) Hay, P. J.; Wadt, W. R. *J. Chem. Phys.* **1985**, *82*, 270.
- (70) Wadt, W. R.; Hay, P. J. *J. Chem. Phys.* **1985**, *82*, 284.
- (71) Hay, P. J.; Wadt, W. R. *J. Chem. Phys.* **1985**, *82*, 299.
- (72) Dennington, R., II; Keith, T.; Millam, J. *GaussView*, Version 4.1.2; Semichem, Inc.: Shawnee Mission, KS, 2007.
- (73) O'Boyle, N. M.; Tenderholt, A. L.; Langer, K. M. *J. Comput. Chem.* **2008**, *29*, 839.
- (74) Sheldrick, G. M. *SHELXS-97, Program for Crystal Structure Solution*; Universität Göttingen: Germany, 1997.
- (75) (a) Sheldrick, G. M. *SHELXL-97, Program for Crystal Structure Refinement*; Universität Göttingen: Germany, 1997. (b) Sheldrick, G. M. *Acta Crystallogr.* **2008**, *A64*, 112.